BRNO UNIVERSITY OF TECHNOLOGY

Faculty of Electrical Engineering
and Communication

MASTER'S THESIS

Brno, 2020 Bc. Iveta Lolová

BRNO UNIVERSITY OF TECHNOLOGY
VYSOKÉ UČENÍ TECHNICKÉ V BRNĚ

FACULTY OF ELECTRICAL ENGINEERING AND COMMUNICATION
FAKULTA ELEKTROTECHNIKY
A KOMUNIKAČNÍCH TECHNOLOGIÍ

DEPARTMENT OF POWER ELECTRICAL AND ELECTRONIC ENGINEERING
ÚSTAV VÝKONOVÉ ELEKTROTECHNIKY A ELEKTRONIKY

TOPOLOGY OPTIMIZATION OF THE LINE-START SYNCHRONOUS MACHINES
TOPOLOGICKÁ OPTIMALIZACE SYNCHRONNÍCH STROJŮ SPOUŠTĚNÝCH ZE SÍTĚ

MASTER'S THESIS
DIPLOMOVÁ PRÁCE

AUTHOR — **Bc. Iveta Lolová**
AUTOR PRÁCE

SUPERVISOR — **Ing. Jan Bárta, Ph.D.**
VEDOUCÍ PRÁCE

BRNO 2020

BRNO UNIVERSITY OF TECHNOLOGY
FACULTY OF ELECTRICAL ENGINEERING AND COMMUNICATION

Master's Thesis

Master's study field **Power Electrical and Electronic Engineering**

Department of Power Electrical and Electronic Engineering

Student: Bc. Iveta Lolová ***ID:*** 186056

Year of study: 2 ***Academic year:*** 2019/20

TITLE OF THESIS:

Topology optimization of the line-start synchronous machines

INSTRUCTION:

1. Review of the state-of-the-art
2. Analyzing possible concepts for characterizing the investigated design space
3. Optimization of line-start synchronous machine
4. Discussion of the results

RECOMMENDED LITERATURE:

[1] PYRHONEN, J.; JOKINEN t.; HRABOVCOVÁ V. Design of rotating eletrical machines. John Wiley and Sons, 2007. ISBN 978-0-470-69516-6.

[2] J.R. HENDERSHOT, T.J.E. MILLER . Design of Brushless Permanent-Magnet Machines. Motor Design Books LLC; Second Edition edition, 2010. ISBN 978-0984068708.

[3] A. E. Fitzgerald, Ch. Kingsley, S. Umans "Electric Machinery", McGrow-Hill Companies Inc., 2003. 688 s. ISBN 0-07-112193-5

Date of project specification: 3.2.2020 ***Deadline for submission:*** 1.6.2020

Supervisor: Ing. Jan Bárta, Ph.D.

doc. Ing. Ondřej Vítek, Ph.D.
Subject Council chairman

WARNING:
The author of the Master's Thesis claims that by creating this thesis he/she did not infringe the rights of third persons and the personal and/or property rights of third persons were not subjected to derogatory treatment. The author is fully aware of the legal consequences of an infringement of provisions as per Section 11 and following of Act No 121/2000 Coll. on copyright and rights related to copyright and on amendments to some other laws (the Copyright Act) in the wording of subsequent directives including the possible criminal consequences as resulting from provisions of Part 2, Chapter VI, Article 4 of Criminal Code 40/2009 Coll.

Abstract

The master thesis deals with topology optimization of electrical machines and line-start synchronous reluctance motor. The master thesis includes a literature review on the state of the art of topology optimizations and line-start synchronous reluctance motor. The possible concepts for characterizing the investigated design space is described. The dependency of the final normalized Gaussian network on the distribution of Gaussian functions is analysed in detail. The evaluation algorithm of a single individual is created within this thesis. The algorithm manages communication between Ansys Maxwell and software tool SyMSpace. Moreover, the algorithm leads to reducing of the computational time due to the preselection of unfeasible geometries. Furthermore, the topology optimization of LSSynRM based on the normalized Gaussian network is performed and the results are discussed.

Keywords

the normalized Gaussian network, topology optimization, line-start synchronous reluctance motor, SyMSpace, Ansys Maxwell, FEM, Pareto front

Abstrakt

Diplomová práce se zabývá topologickou optimalizací elektrických strojů a reluktančními synchronními stroji spouštěnými za sítě. Práce obsahuje literární rešerši na téma topologické optimalizace elektrických strojů a na téma synchronní reluktanční stroj spouštěný ze sítě. Jsou zde popsány možné způsoby charakterizace optimalizovaného prostoru. Především je rozebrán vliv rozmístění Gaussových funkcí na finální Gaussovu síť. V této práci je vytvořen vyhodnocovací algoritmus pro jednotlivé jedince, který zajišťuje komunikaci mezi Ansys Maxwell a optimalizačním softwarem SyMSpace. Navíc tento algoritmus vede ke zkrácení výpočetní doby počáteční selekcí nevyhovujících jedinců. Dále je provedena topologická optimalizace LSSynRM s využitím normalizované Gaussovy sítě a zhodnocení výsledků.

Klíčová slova

normalizovaná Gaussova síť, topologické optimalizace, synchronní reluktanční motor spouštěný ze sítě, SyMSpace, Ansys Maxwell, FEM, Pareto front

Rozšířený abstrakt

Diplomová práce se zabývá topologickou optimalizací synchronních strojů spouštěných ze sítě. Topologická optimalizace (TO) nabízí novou možnost pro zlepšení vlastností elektrických strojů. V první kapitole této práce je TO srovnána s parametrickou optimalizací. Bylo zjištěno, že hlavní výhodou TO je finální geometrie, která je oproštěna téměř jakýchkoliv předešlých omezení. Přičemž v tomto ohledu tato geometrie může nabídnout vhodnější řešení pro zadaný specifický úkol jako je maximalizace momentu či účinnosti, než by nabídla parametrická optimalizace.

Dále byla provedena literární rešerše na téma synchronních reluktančních strojů spouštěných ze sítě, které byly shledány jako vhodnou náhradou pro méně účinné, hojně využívané asynchronní stroje. V druhé kapitole je popsána konstrukce a princip činnosti, včetně matematického popisu.

Třetí kapitola se již zabývá možnými koncepty pro charakterizování optimalizovaného prostoru během TO. Optimalizovaný prostor je rozdělen na dílčí elementy, přičemž každému může být přiřazen materiál nezávisle na ostatních elementech. V této kapitole je přímé přiřazovaní materiálů jednotlivým prvkům zavrhnuto a je využito metody přiřazovaní materiálů na základě normalizovaných Gaussových sítí (NGnet). Je zde podrobně popsána tvorba normalizované Gaussovy sítě, především vliv rozložení jednotlivých Gaussových funkcí na finální NGnet.

Poslední kapitola popisuje TO s využitím NGnet v optimalizačním nástroji SyMSpace. Je zde popsán největší přínos této diplomové práce, a to vytvoření vyhodnocovacího algoritmu pro jednotlivé jedince v TO. Vytvořený algoritmus zajišťuje komunikaci mezi SyMSpace a programem Ansys Maxwell. Navíc tento algoritmus vyselektuje nerealizovatelné či neslibné geometrie, ještě před provedením časově náročné transientní analýzy. Algoritmus je rozdělen na tři části. V první části algoritmus se zjišťuje proveditelnost geometrie pomocí hledání celistvé plochy. Pokud je geometrie vyhodnocena jako nerealizovatelná, je algoritmus ukončen a jedinec je vyselektován jako nevyhovující. V druhé části probíhá kontrola momentu v ustáleném stavu, kdy opět geometrie a její vlastnosti mohou být označeny za nevyhovující. Třetí a poslední částí je provedení transientní analýzy. Hlavní výhodou tohoto algoritmu je významná redukce času vyhodnocení nevyhovující geometrie z přibližných 2-3 hodin při samotném použití transientní analýzy na 5-30 minut v závislosti na tom, v které části je geometrie vyselektována. Je zde provedeno zhodnocení výsledků dosažených z provedené TO. Na základě těchto výsledků práce uvádí doporučení pro budoucí zlepšení, jak v části při přípravě NGnet v závislosti na rozložení jednotlivých Gaussových funkcí, tak v části samotného nastavení optimalizačního procesu.

Bibliographic citation:

LOLOVÁ, Iveta. *Topology optimization of the line-start synchronous machines*. Brno, 2020. Online: https://www.vutbr.cz/studenti/zav-prace/detail/125799. Master's Thesis. Brno University of Technology, Faculty of electrical engineering and communication, Department of Power Electrical and Electronic Engineering. Supervisor: Jan Bárta.

Bibliografická citace:

LOLOVÁ, Iveta. *Topologické optimalizace elektrických strojů* [online]. Brno, 2020. Dostupné z: https://www.vutbr.cz/studenti/zav-prace/detail/123297. Diplomová práce. Vysoké učení technické v Brně, Fakulta elektrotechniky a komunikačních technologií, Ústav výkonové elektrotechniky a elektroniky. Vedoucí práce: Jan Bárta.

Declaration

I declare that I have written the Master Thesis titled "Topology optimization of the line-start synchronous machines" independently, under the guidance of the advisor and using exclusively the technical references and other sources of information cited in the thesis and listed in the comprehensive bibliography at the end of the thesis.

As the author I furthermore declare that, with respect to the creation of this Master Thesis, I have not infringed any copyright or violated anyone's personal and/or ownership rights. In this context, I am fully aware of the consequences of breaking Regulation § 11 of the Copyright Act No. 121/2000 Coll. of the Czech Republic, as amended, and of any breach of rights related to intellectual property or introduced within amendments to relevant Acts such as the Intellectual Property Act or the Criminal Code, Act No. 40/2009 Coll., Section 2., Head VI., Part 4.

Prohlášení

Prohlašuji, že svou diplomovou práci na téma "Topologická optimalizace synchronních strojů spouštěných ze sítě" jsem vypracovala samostatně pod vedením vedoucího diplomové práce a s použitím odborné literatury a dalších informačních zdrojů, které jsou všechny citovány v práci a uvedeny v seznamu literatury na konci práce.

Jako autorka uvedené diplomové práce dále prohlašuji, že v souvislosti s vytvořením této diplomové práce jsem neporušila autorská práva třetích osob, zejména jsem nezasáhla nedovoleným způsobem do cizích autorských práv osobnostních a jsem si plně vědoma následků porušení ustanovení § 11 a následujících autorského zákona č. 121/2000 Sb., včetně možných trestněprávních důsledků vyplývajících z ustanovení části druhé, hlavy VI. díl 4 Trestního zákoníku č. 40/2009 Sb.

V Brně dne …….. Podpis autora ……..

Acknowledgement

This work has been supported by the COMET-K2 Center of the Linz Center of Mechatronics (LCM) funded by the Austrian federal government and the federal state of Upper Austria.

I am sincerely grateful to my supervisor Ing. Jan Bárta, Ph.D. for professional guidance, consultation, patience and invaluable suggestions for the work.

I would like to thank Dipl.-Ing Dr. Gerd Bramerdorfer for providing me with helpful literature and advice at the beginning and during of the research and for training in SyMSpase.

Next thanks go to Brno University of Technology, Johannes Kepler University and AKTION Czech Republic-Austria scholarship for my whole studies and the possibility of my stay at Johannes Kepler University in Linz.

My warm thanks to my husband Ing. Martin Lola for his infinite patience, love and support during my whole studies. I thank my family and all my friends.

Poděkování

Tato práce byla podpořena Centrem mechatronicky v Linci (LCM) COMET-K2 financovaného Rakouskou spolkovou vládou a spolkovou zemí Horní Rakousko.

Děkuji vedoucímu diplomové práce Ing. Janu Bártovi, Ph.D. za účinnou metodickou, pedagogickou a neocenitelnou odbornou pomoc a další cenné rady při zpracování mé diplomové práce.

Ráda bych poděkovala Dipl.-Ing Dr. Gerdu Bramerdorferovi za poskytnutí literatury a rad na začátku a během celé práce a také za kurz v programu SyMSpace.

Dále bych chtěla poděkovat Vysokému Učení Technickému v Brně, Univerzitě Johanna Keplera v Linci a projektu Aktion Česká Republika-Rakousko za celé mé studium a umožnění mého pobytu na Univerzitě Johanna Keplera v Linci.

Vřele bych chtěla poděkovat mému manželovi Ing. Martinu Lolovi za jeho nekonečnou trpělivost, lásku a podporu během celého mého studia. Děkuji své rodině a všem přátelům.

Contents

List of figures 1
List of tables 3
Abbreviations and Symbols 4
Introduction 7
1 Topology optimization 8
1.1 Introduction and motivation 8
1.2 Optimization algorithms 10
1.2.1 Stochastic algorithms 10
1.2.2 Evolutionary algorithms 11
1.3 Topology optimization method 13
1.4 The ON/OFF method 13
2 Line-start synchronous reluctance machine 15
2.1 Construction 15
2.2 The operation principle of LSSynRM 16
2.2.1 The asynchronous starting process 17
2.3 Mathematical description 18
2.4 Pull-in torque 21
2.5 Current solutions 21
3 The characterizing the investigated design space 23
3.1 The optimized motor and its investigated design space 23
3.2 The normalized Gaussian network (NGnet) 25
3.3 Deployment of Gaussian functions in NGnet 27
3.3.1 First version of distribution of Gaussian functions 27
3.3.2 Second version of distribution of Gaussian functions 29
3.3.3 Variance and overleap 30
3.3.4 Final version of distribution of Gaussian functions 32
4 Topology optimization of line-start synchronous reluctance motor 35
4.1 SyMSpace project for topology optimization of LSSynRM 36
4.2 SyMSpace Optimizer setting 37
4.3 Evaluation algorithm of single individual 39
4.3.1 Geometry check 39
4.3.2 Torque check 43

4.3.3 Transient analysis 43
4.4 Results of optimization 44
4.5 The optimized LSSynRM 47
4.5.1 Starting process 51
4.5.2 Behavior at steady-state 53
4.5.3 Comparison of optimized LSSynRM with prototypes showed in [4] 57
Conclusion 60
References 62

List of figures

1.1 Example of two cross-sections of rotor designs. Light green parts denote iron elements and dark blue parts denote air gaps [5]. 9
1.2 Rotor designs obtained by DECMO (with a real-value encoding) for the realistic DTO scenario [5]. 9
1.3 The genetic algorithms model. 12
1.4 Crossover operation to generate offspring and mutation of generated offspring. 13
1.5 The optimized rotor shape from [15]. 14
1.6 Resultant rotor shapes for three Gaussian distribution (see also Fig. 3.10a) [16]. 14
2.1 Synchronous reluctace rotor [17]. 15
2.2 SynRM rotor types: a) Salient pole rotor, b) Axially Laminated Anisotropic (ALA) rotor, c) Transversely Laminated Anisotropic (TLA) rotor [3]. 16
2.3 Cross section of one pole of 4-pole SynRM rotors.a) Basic SynRM geometry. b) LSSynRM rotor with Full barriers Filling (FuF); c) LSSynRM rotor with Partial barriers Filling (PaF) [18]. 16
2.4 Structure of LSSynRM based on induction motor presented in [20], [21] and [22]. 17
2.5 Asynchronous torque in half-speed range [3]. 18
2.6 The d-q axis reference. 19
2.7 Equivalent circuit of LSSynRM in dq-coordinate system [3]. 19
2.8 The selected topologies of geometries presented in [3]. 21
2.9 Cross-sections of geometries of 4-pole 30 kW LSSynRMs [25]. 22
2.10 Topology of 2-pole 2.2 kW LSSynRM [20]. 22
2.11 Topology of the LSSynRM presented in patent [27]. 22
3.1 The created model in Ansys Maxwell for topology optimization. . . . 24
3.2 The normalized Gaussian function $G(x, y)$. 24
3.3 The normalized Gaussian network $f(x, y)$. 25
3.4 The Gaussian functions and their sum. 26
3.5 The normalized Gaussian network defines final geometry. 27

3.6 The deployment of (9) Gaussian functions. 28
3.7 First distribution of Gaussian functions. 28
3.8 Second distribution of Gaussian functions. 29
3.9 Deployment dependency on variance σ and overleap Ω. 31
3.10 Comparison of the different Gaussians distributions in paper [16]. . . 32
3.11 The comparison of symmetrical (a) (c) and asymmetrical NGnet (b) (d). 33
3.12 Alternation of asymmetrical NGnet into symmetrical NGnet. 34
4.1 Graphical user interface of the simulation framework SyMSpace [28]. 35
4.2 Prepared SyMSpace project for topology optimization of LSSynRM . 37
4.3 Evaluation algorithm of one individual. 40
4.4 NGnet transformation into matrix defining the elements. 41
4.5 The geometry test algorithm. 42
4.6 Memory archive in SyMSpace Optimizer. 44
4.7 Torque ripple vs efficiency. 45
4.8 Torque ripple vs power factor. 46
4.9 Power factor vs efficiency. 46
4.10 The geometry of the optimized LSSynRM for the detailed analysis. . . 47
4.11 Mesh grid of the model in Ansys Maxwell. 48
4.12 Phasor diagram at steady-state. 49
4.13 Distribution of losses. 50
4.14 Losses behavior at steady-state. 50
4.15 Speed dependency on time during the starting process. 51
4.16 Torque dependency on time during the starting process. 51
4.17 Torque dependency on speed. 52
4.18 Phase currents dependency on time during the starting process. . . . 52
4.19 Flux density distribution in the LSSynRM. 53
4.20 Magnetic flux density in the middle of the air gap. 54
4.21 Normalized harmonic content of flux density normal component. . . 54
4.22 Currents behavior at steady-state. 55
4.23 Normalized harmonic content of the phase current. 55
4.24 Torque behavior at steady-state. 56
4.25 Normalized harmonic content of torque. 56
4.26 Load angle vs torque. 57
4.27 The geometries selected for comparison. 58

List of tables

3.1 Specification of the optimized motor. 23
3.2 Settings of variance and overleap. 30
4.1 Optimized parameters setting. 38
4.2 Objectives and constraints setting. 38
4.3 Main parameters of LSSynRM in steady-state. 48
4.4 The distribution of losses in steady-state. 49
4.5 Comparison of optimized LSSynRM, initial IM and LSSynRMs [4]. . . 58

Abbreviations and Symbols

Symbol	Meaning	Unit
b_i	Component of the function of the NGnet	[-]
B_{rad}	Fundamental harmonic of flux density	[T]
$cos\varphi$	Power factor	[-]
f	the function of the NGnet	[-]
G	Gaussian function	[-]
i_d	Stator current in d-axis, instantaneous value $i(t)$	[A]
i_q	Stator current in q-axis, instantaneous value $i(t)$	[A]
i_D	Damper winding (rotor) current in d-axis, instantaneous value $i(t)$	[A]
i_Q	Damper winding (rotor) current in q-axis, instantaneous value $i(t)$	[A]
I_1n	Rated phase current	[A]
J_m	Motor moment of inertia	[kg m2]
J_{load}	Load moment of inertia	[kg m2]
J_{tot}	Accounts for the motor and load moment of inertia	[kg m2]
L_d	Synchronous inductance in d-axis	[H]
L_q	Synchronous inductance in q-axis	[H]
L_{md}	Magnetizing inductance in d-axis	[H]
L_{mq}	Magnetizing inductance in q-axis	[H]
$L_{s\sigma}$	Stator winding leakage inductance	[H]
$L_{D\sigma}$	Damper winding leakage inductance in d-axis	[H]
$L_{Q\sigma}$	Damper winding leakage inductance in q-axis	[H]
n	Rated speed	[rpm]
N	Number of Gaussian functions	[-]
p	Number of pole pairs	[-]
P_1	Rated input power	[W]
P_2	Rated output power	[W]
P_{CuS}	Stator resistive losses	[W]
P_{Extra}	Extra losses	[W]
P_{Fe}	Iron losses	[W]
P_{Mech}	Mechanical losses	[W]
P_{Solid}	Solid losses	[W]
P_{Sum}	Sum of losses	[W]

R_s	Stator resistance	[Ω]
R_D	Damper winding (rotor) resistance in d-axis	[Ω]
R_Q	Damper winding (rotor) resistance in q-axis	[Ω]
s	Slip	[-]
S	Apparent power	[VA]
u_d	Stator voltage in d-axis, instantaneous value $u(t)$	[V]
u_q	Stator voltage in q-axis, instantaneous value $u(t)$	[V]
U_n	Line-to-line voltage	[V]
T_{cage}	Asynchronous component of the electromagnetic torque	[Nm]
T_{em}	Electromagnetic torque	[Nm]
T_{load}	Load torque	[Nm]
T_n	Rated torque	[Nm]
T_{rel}	Synchronous component of the electromagnetic torque	[Nm]
T_{ripple}	Torque ripple peak to peak	[Nm]
T_{ripple}	Torque ripple	[%]
w_i	Weighting coefficient of the function of the NGnet	[-]
δ	Load angle	[°]
η	Estimated efficiency from losses	[%]
η_1	Estimated electromagnetic efficiency from losses	[%]
η_2	Estimated efficiency from input/output ratio	[%]
μ	Expected value/Position of the Gaussian function	[-]
μ_x	Expected value/Position of the Gaussian function in x-axis	[-]
μ_y	Expected value/Position of the Gaussian function in y-axis	[-]
σ	Variance of the Gaussian function	[-]
σ_x	Variance of the Gaussian function in x-axis	[-]
σ_y	Variance of the Gaussian function in y-axis	[-]
Ψ_d	stator magnetic flux linkage space vector in d-axis	[Wb]
Ψ_q	stator magnetic flux linkage space vector in q-axis	[Wb]
Ψ_D	Damper winding (rotor) magnetic flux linkage space vector in d-axis	[Wb]
Ψ_Q	Damper winding (rotor) magnetic flux linkage space vector in q-axis	[Wb]

Ψ_{md}	Air-gap magnetic flux linkage space vector in d-axis	[Wb]
Ψ_{mq}	Air-gap magnetic flux linkage space vector in q-axis	[Wb]
ω_{nc}	Angular frequency of negative component of the flux	[rad/s]
ω_{pc}	Angular frequency of positive component of the flux	[rad/s]
ω_r	Electrical angular frequency of rotor	[rad/s]
ω_s	Electrical synchronous angular frequency	[rad/s]
Ω	Overleap of deployed Gaussian function	[-]
Ω_{rmech}	Mechanical angular frequency of rotor	[rad/s]

Abbreviation	**Meaning**
ALA	Axially Laminated Anisotropic (rotor)
DECMO	Differential evolution-based the coevolutionary multi-objective optimization algorithm
DTO	Direct topology optimization
EF	Efficiency
FEA	Finite element analysis
FEM	Finite element method
FFT	Fast Fourier transform
GA	Genetic algorithm
IM	Induction motor
LS	Local search
LSSynRM	Line-start synchronous reluctance motor
MOEA	Multi-objective evolutionary algorithm
NGnet	The normalized Gaussian network
NSGA-II	The non-dominated sorting genetic algorithm II
PF	Power factor
SPEA2	The strength Pareto evolutionary algorithm
SynRM	Synchronous reluctance motor
THD	Total harmonic distortion
TLA	Transversely Laminated Anisotropic (rotor)
TR	Torque ripple

Introduction

The world focuses on energy saving more than ever due to economic and climatic reasons. The electrical motors represent the larger consumers of electricity in the industrial sector and also in the tertiary sector. The electric motors consume about 40 % of generated electricity [1]. The most commonly used kind of the motor is induction motor, because of its low production cost, simple manufacturing and satisfactory features. Thus, the induction motors represent one of the greatest energy consumption apparatuses worldwide [2]. The opportunity of reducing electricity consumption is one of the reasons for the chosen topic of this master thesis.

This master thesis deals with topology optimization of the line-start synchronous machines. The topology optimization offers a new way to the machines performance improvement. The comparison between direct topology optimization and shape optimization also called as the parametric optimization, is presented in the first chapter. There is also a brief description of optimization algorithms, especially evolutionary algorithms. The topology optimization technique the ON/OFF method is presented.

The line-start synchronous reluctance machine is chosen as the possible replacement of induction motors with reducing electricity consumption goal in this master thesis. The second chapter describes the construction and operation principle of such a motor. The LSSynRM is a hybrid of induction motor and synchronous reluctance motor and it joints the positive feature from both of them [3]. Furthermore, the second chapter deals with the mathematical description of LSSynRM.

The third chapter presents the analysis of possible concepts for characterizing the investigated and optimized design space. Firstly the created model in Ansys Maxwell is described and the theory of the normalized Gaussian network is explained. This chapter mainly focuses on the deployment of Gaussian functions in the normalized Gaussian network.

Topology optimization of line-start synchronous reluctance motor based on the normalized Gaussian network is described in the last chapter. This chapter includes a description of SyMSpace project for topology optimization of LSSynRM and also a description of SyMSpace Optimizer setting which is used during optimization in this master thesis. The main part of this chapter deals with the created evaluation algorithm of a single individual. This algorithm must be created in this thesis, because the transient analysis, which is required for analysis LSSynRM, demands an enormous amount of time. Further, the last chapter present Pareto front obtained by the topology optimization, which ran for one and half month. The one individual is picked for thoughtful analysis. There is a comparison of the LSSynRM with equal rated output power presented in [4].

1 Topology optimization

1.1 Introduction and motivation

Electrical motor represents one of the greatest energy consumption apparatuses in the world. We should deal with the optimization of electrical rotating machines because there are worldwide efforts for reducing energy consumption.

According to [5] there are different approaches to electrical machine design optimization. The standard approach is a parametric optimization. An expert in the field selects a machine topology and creates a parametric model. Electrical machine design optimization is then done by finding ideal parameters for the preselected topology. Although the selection of suitable topology is a crucial step, it is in the hand of the designer. The selection of topology is crucial because selected topology has a direct impact on the results we obtain from parametric optimization. Any good results will not be obtained from any amount of optimization if the wrong parametrized topology for optimization is chosen.

The second approach to electrical machine design optimization is direct topology optimization (DTO). In this case, the design space is discretized into small elements creating a grid. Each element can be independently assigned with particularly defined material properties (i.e., electrical steel, aluminium, copper etc.). If we choose the simplest variation consisting of only two materials: iron-air or iron-aluminium, number of possible designs is 2^n, where n is the number of elements. Thus, computational effort significantly increases and restrictions must be implemented to avoid unreasonable geometries. On the other hand, the definition of the machine's structure is much more flexible and, thus, we could reach a better performance of optimized motors [5]. Figure 1.1 shows an example of two cross-sections of rotor designs. Fig. 1.1a shows the first rotor design based on the parametric model. The second rotor design based on a discrete grid is shown in Fig. 1.1b.

The topology optimization also brings another advantage. There are not required experience of a designer (an expert in the field). It is meant in the way that for creating a parametric model the designer should already know how the geometry of rotor influence the performance of the motor. For example, the maximum output power is required of the optimized synchronous reluctance motor. The parametric model must be created for parametric optimization, but it is almost impossible for the designer to know the best geometry before the optimization is done. The designer must choose the geometry, e.g. the number of the flux barriers and their shape. The parametric optimization of the parametrized geometry, of course, leads to the ideal parameters of parametrized geometry for the maximum output power. The problem is that the initial parametrized geometry does not have to lead to the best rotor geometry to maximize output power

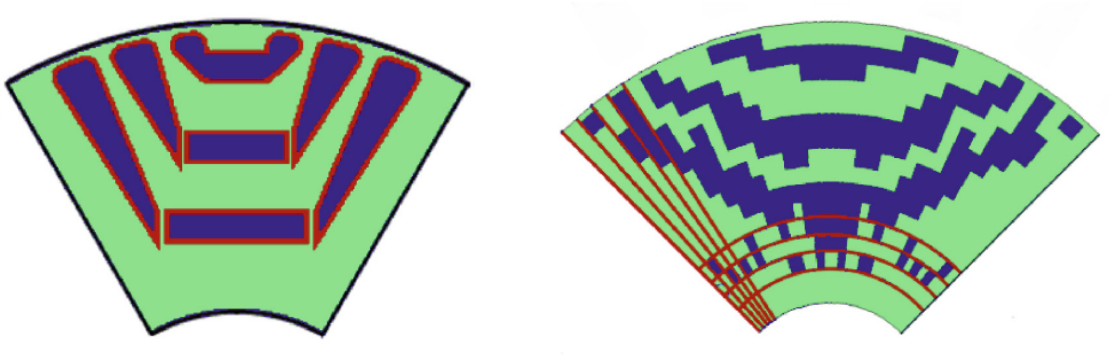

(a) Based on parametric model.

(b) Based on discrete grid.

Figure 1.1: Example of two cross-sections of rotor designs. Light green parts denote iron elements and dark blue parts denote air gaps [5].

and there could exist most suitable geometries for that task. The DTO offers a better solution for this task. The DTO creates/choose the best geometry of the rotor without any previous limitations (e.g. defining a number of the flux barriers etc.).

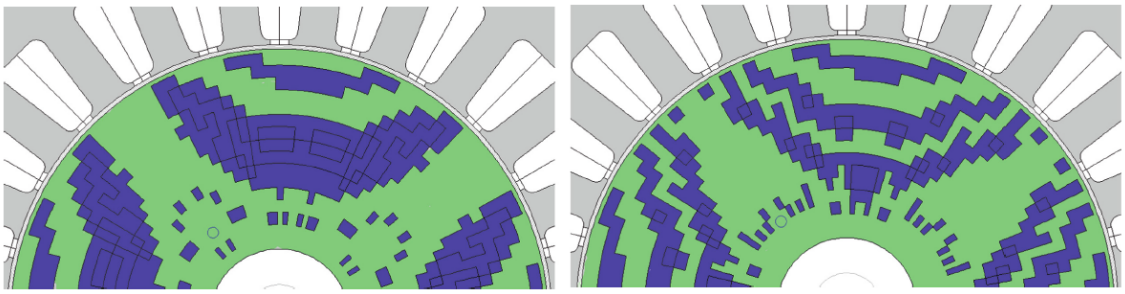

(a) Design that maximize output power.

(b) Design that minimize torque ripple.

Figure 1.2: Rotor designs obtained by DECMO (with a real-value encoding) for the realistic DTO scenario [5].

In [5] the direct topology optimization for maximum output power and the direct topology optimization for minimum torque ripple were performed. The fitness assessments were performed via finite element simulations and multi-objective evolutionary algorithm (MOEA): DECMO was used for the DTO scenarios. The examples of two cross-sections of the two rotor designs obtained by DECMO are shown in Fig. 1.2. The first rotor design that maximizes the output power of the motor is shown in Fig. 1.2a. The two flux barriers are present in the geometry of this rotor. In Fig. 1.2b is the second rotor design that minimizes torque ripple. The three flux barriers are present in the geometry of this rotor. Thanks to the DTO the best rotor design were created for each task. If the parametric model with three flux barriers is used in parametric optimization for maximizes output power, the motor would not reach the same power as the one created

by the DTO. On the other hand, the geometry of the rotor, created by parametric optimization, has a smoother shape than the one created by the DTO. At this moment the designer knows the number of flux barriers that maximizes output power thanks to DTO and, thus, the designer can create the new parametric model based on the preliminary rotor geometry created by the DTO. Now, this parametric model can reach the ideal rotor geometry that maximizes output power.

1.2 Optimization algorithms

Optimization algorithms are great tools for resolving many problems. The optimization algorithms are used for resolving problems, that can not be solved by analytical method. Thus, finding an analytical model is very complicated or impossible. Most of the technical problems can be defined as a optimization problem, thus, a mathematical problem [6]. After defining the problem into a function with parameters, the arguments can be found by optimization. This step is also called defining the cost function. The optimization process is finding a global minimum of the cost function which described single-objective optimization

$$minimize f(\mathbf{x}), \tag{1.1}$$

where $\mathbf{x} \in$ D, D is called domain of definition of a function or search space and $\mathbf{x}$ are parameters of the cost function. Finding a global maximum of the cost function is defined:

$$maximize f(\mathbf{x}) = minimize(-f(\mathbf{x})) \tag{1.2}$$

The global minimum x_0 of function f($\mathbf{x}$) is defined as:

$$f(x_0) \leq f(\mathbf{x}) \tag{1.3}$$

In topology optimization of electrical machines, the objective value of the cost function for the design of the electrical machine can be obtained by evaluating a complex analysis which includes a finite element simulation.

1.2.1 Stochastic algorithms

The stochastic algorithms are used when a determined algorithm solving the problem can not be found. The stochastic algorithms do not always find a solution to the problem with a determined count of steps, but they find often the solution in optimal time [7]. The stochastic algorithms solving a global optimization use heuristic methods for space searching. Heuristics is a process that uses chance, intuition, analogy and experience

[8]. The difference between heuristics and deterministic algorithms is that, unlike the deterministic algorithms, heuristics do not always provide a solution.

Most stochastic algorithms for finding the global minimum or maximum contain a learning process. The inspirations for using heuristics are often derived from knowledge of natural or social processes [7]. E.g. ants find the shortest route to a source of food [9] or wolf packs searching for food [6] or competitive–cooperative behaviour of a pack of intelligent agents [10]. These are just three examples of many. Similar learning techniques can be found in all known stochastic algorithms except for blind random search. In recent decades, stochastic algorithms, especially of the evolutionary type, have been used with relative success for finding a global minimum of functions. A detailed description of this issue can be found for example in the books [7], [11] and [12].

1.2.2 Evolutionary algorithms

Evolutionary algorithms are a summarizing term for various approaches using models of evolutionary processes for purposes that have almost nothing in common with biology. It tries to use ideas of the driving forces of the evolution of living matter for optimization purposes [7]. Evolutionary algorithms are primarily used to solve large complex optimization problems with many local optimizations because there is less chance of getting stuck at a local minimum than with traditional gradient methods. Evolutionary algorithms are much more robust and more complex than other search algorithms.

It is characteristic of them that they work with the population and use heuristics, which in some way modify the population to improve its properties. Evolutionary algorithms have been and are the subject of intensive research and the number of publications in this field is very large. One of the main motives is applications in practical problems, which are not solvable by other methods e.g. grid analysis, gradient methods etc. The development of evolutionary algorithms is mainly a matter of recent decades and is caused by the development of computers and advances in computer science.

The genotype contains genes and usually encodes one (but could encode more) phenotype, thus, candidate for solving the problem of the relevant domain of a solution, e.g. dimensions of space slot for aluminium in line-start synchronous reluctance motor or the precise geometry of the rotor. During encoding, the genes of numerical values acquire values from the corresponding domain. So the genotype can be transformed into the appropriate phenotype in the decoding process. The entire decoding process should be easy to perform. The phenotype evaluation determines the fitness of the corresponding genotype (individual). Evolutionary algorithms prefer genotypes (individuals) with the highest fitness rating, which are created by operators (e.g. mutation, crossover, selection, inversion etc.) over many generations [7]. According to [11], the individuals in the population compete and exchange information so the population gradually evolves

toward a genotype that corresponds to the largest fitness phenotype, which corresponds to the solution to the problem.

1.2.2.1 Genetic algorithms

Genetic algorithms have been derived from biological genetics and the theory of evolution that affects the evolution of everything living on this planet. Evolutionary algorithms are simple models of Darwin's evolutionary theory of population development. The first evolutionary algorithm is based on the Darwinian principle of the 'survival of the fittest' and the principal of parents and offsprings [9], [13]. The general construction of evolutionary algorithms is shown in Fig. 1.3.

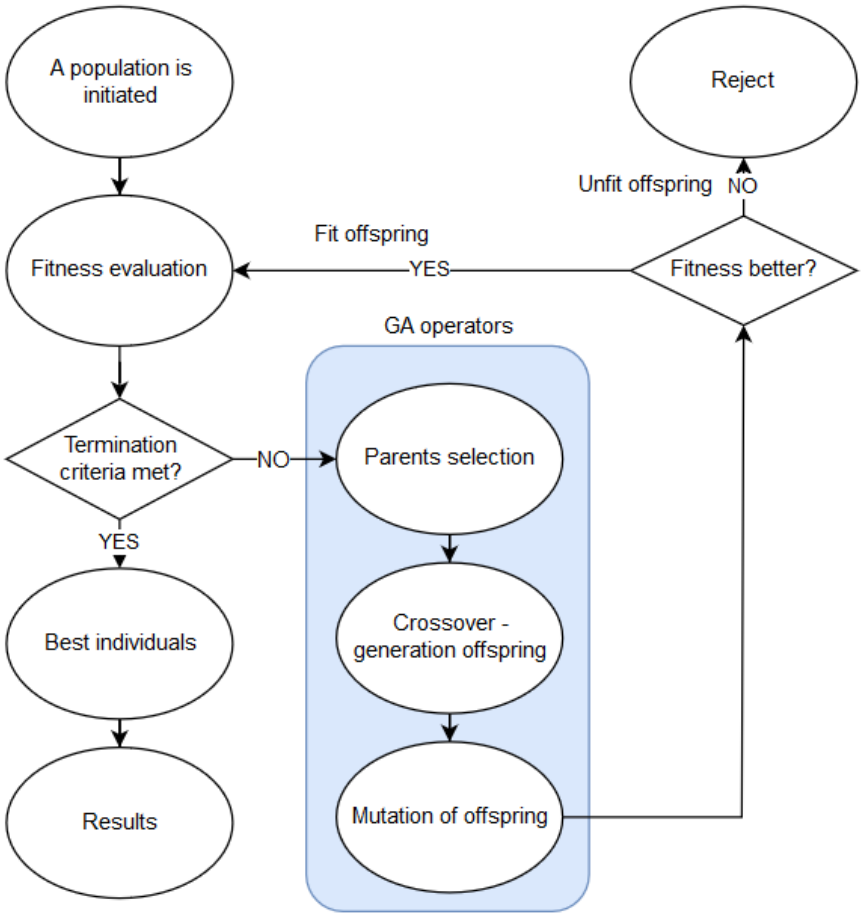

Figure 1.3: The genetic algorithms model.

1.2.2.2 Particle swarm optimization

Particle Swarm Optimization (PSO) is an evolutionary computing technique developed by Eberhart and Kennedy in 1995 [14]. The particle swarm optimization is inspired by the social behaviour of bird and fish flocks. This method has its roots in artificial intel-

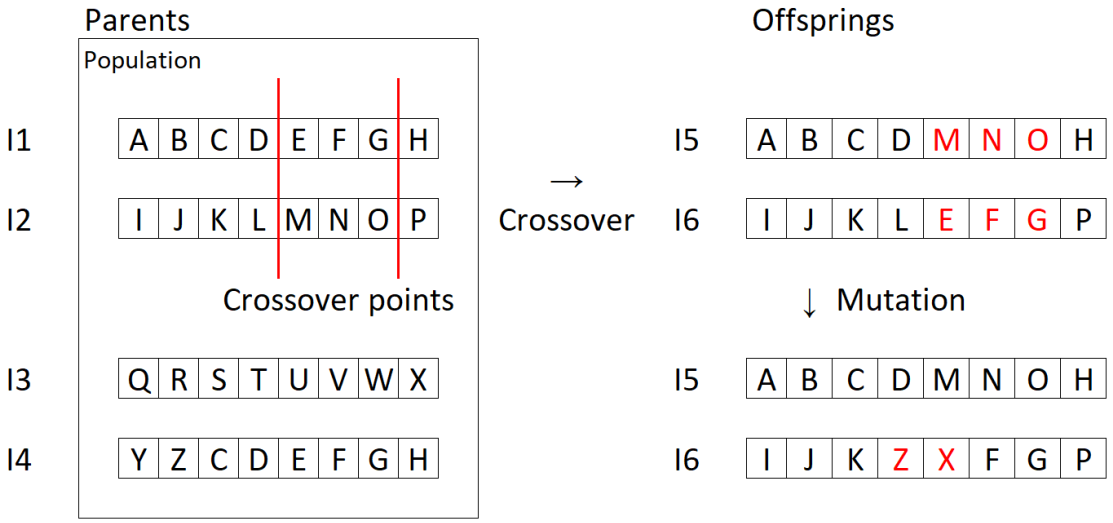

Figure 1.4: Crossover operation to generate offspring and mutation of generated offspring.

ligence or social psychology, as well as in computer science and engineering. PSO uses populations of particles (the bird or fish) that fly through the search area at a certain speed. In each step of the algorithm, this velocity is determined individually for each particle, according to the best particle position and the best particle position of particles in its neighbourhood found during the running of the algorithm [9]. That means the PSO includes intelligence, thus birds use experience from their own experience (local search), and social interaction, thus birds also use the experience of other birds in their neighbourhood (global search) [14]. The best particle position is determined using a user-defined fitness function. The movement of each particle naturally leads to an optimal solution or a solution close to the optimum.

1.3 Topology optimization method

1.4 The ON/OFF method

The ON/OFF method based on the normalized Gaussian network is presented in paper [15]. For this method is typical that computational effort is enormous if there are no restrictions for defining each element. There are 2^n possible geometries with no restrictions defined. The normalized Gaussian network (NGnet) is used for the reduction of possible geometries of ON/OFF method. The ON/OFF method based on the normalized Gaussian network is investigated in [15] for optimization of Synchronous Reluctance motor (SynRM). In Fig. 1.5 the outcomes of topology optimization based on the NGnet can be seen. The ON/OFF method based on the normalized Gaussian network is explained in the third chapter of this master thesis.

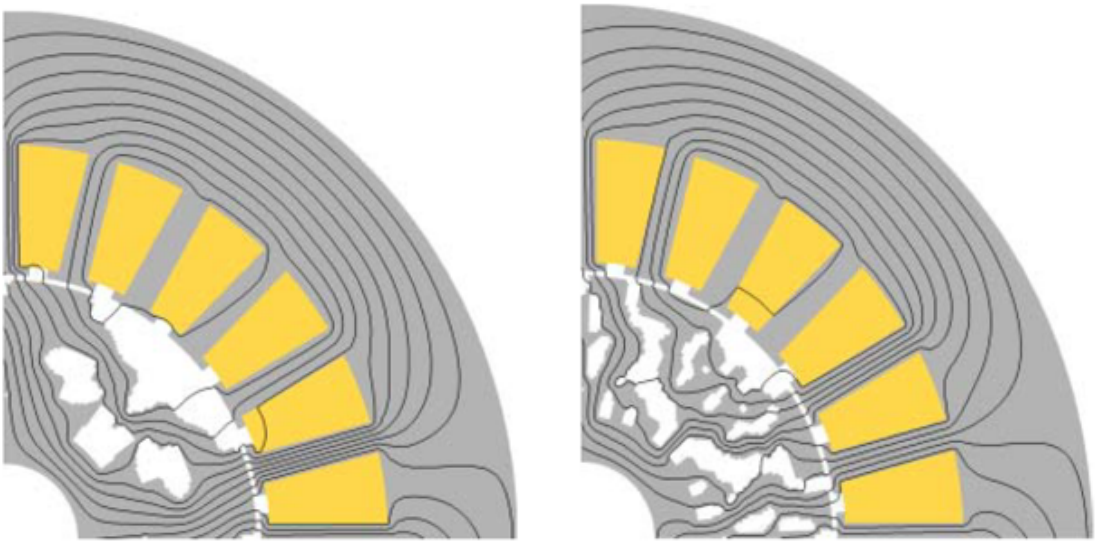

(a) 86 Gaussians. **(b)** 125 Gaussians.

Figure 1.5: The optimized rotor shape from [15].

In [16] using of the normalized Gaussian network for multi-material topology optimization of interior permanent magnet synchronous motor. This method is called the NGnet-based multi-material topology optimization (NGnet-MTO) method. Two NGnets are required for NGnet multi-material topology optimization. Two NGnets are required for NGnet based multi-material topology optimization. Fig. 1.6 shows the results from NGnet based multi-material topology optimization.

Figure 1.6: Resultant rotor shapes for three Gaussian distribution (see also Fig. 3.10a) [16].

2 Line-start synchronous reluctance machine

2.1 Construction

The line-start synchronous reluctance motor has the same stator as an induction motor. The distributed stator winding is commonly used in the stator. The rotor of the LSSynRM is different from induction motor because the LSSynRM rotor must have an anisotropic magnetic structure for synchronous operating. Different magnetic reluctance can be reached in two different ways. Firstly, some of the rotor's teeth can be removed and, thus, rotor with the salient pole is created Fig. 2.1. In Fig. 2.2(a) another type of the salient pole rotor is shown. This approach is not used because of the poor performance of the type of motor. Secondly, the axially laminated anisotropic rotor is created Fig.2.2(b). This type of rotor has problematic manufacturing. Also, due to the flux fluctuation in the laminations, it has additional iron losses [3]. Thirdly, some flux barriers are present in the rotor yoke Fig. 2.2(c). These flux barriers are just air spaces in basic synchronous reluctance machine.

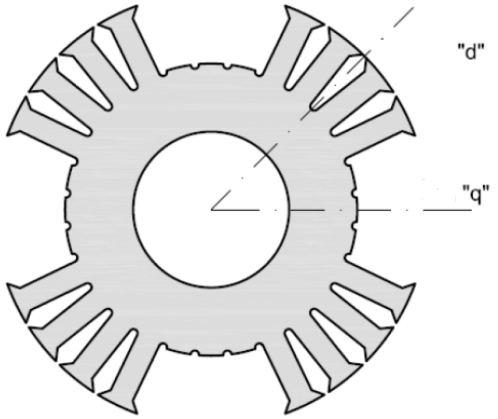

Figure 2.1: Synchronous reluctace rotor [17].

The starting cage has to be implemented into the rotor of SynRM to make it capable to start directly from the line. The Synchronous reluctance motor with the cage winding is called the line-start synchronous reluctance motor(LSSynRM). Then the flux barriers are partially or fully filled with aluminium schematized in Figs. 2.3. These two line-start prototypes were presented in [18] and [19]. Moreover, the LSSynRM with a very similar structure of induction motor, shown in Fig. 2.4, are investigated in papers [20], [21] and [22].

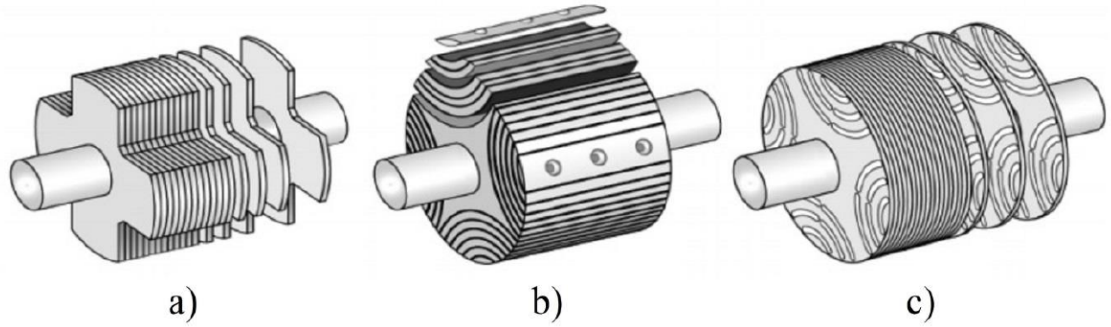

Figure 2.2: SynRM rotor types: a) Salient pole rotor, b) Axially Laminated Anisotropic (ALA) rotor, c) Transversely Laminated Anisotropic (TLA) rotor [3].

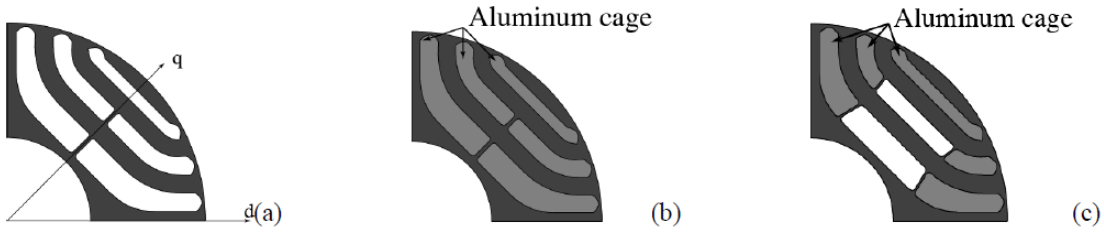

Figure 2.3: Cross section of one pole of 4-pole SynRM rotors.a) Basic SynRM geometry. b) LSSynRM rotor with Full barriers Filling (FuF); c) LSSynRM rotor with Partial barriers Filling (PaF) [18].

2.2 The operation principle of LSSynRM

The LSSynRM is capable to start as an induction machine with a short-circuited rotor cage. Although the LSSynRM works similarly as an induction motor during the starting process, there are differences due to the variable magnetic reluctance in direct- and quadrature-axis in rotor structure. The ratio of inductances in d-axis and q-axis is called a saliency ratio. Because of the saliency ratio, the starting process will be slightly different from an induction machine. After connecting stator winding to the line, the three-phase currents create a rotating magnetic field in an air gap. The rotor starts to rotate due to an induced voltage in the short-circuited cage, which creates the currents in the cage. When the rotation speed is close to the synchronous speed, thus the slip approaches zero, the motor jumps to synchronism [23], [24]. Slip is defined exactly as in an asynchronous motor (2.1). Thus, there are three different operation states of LSSynRM:

1. Asynchronous starting process (asynchronous run-up)
2. Synchronization
3. Synchronous steady-state

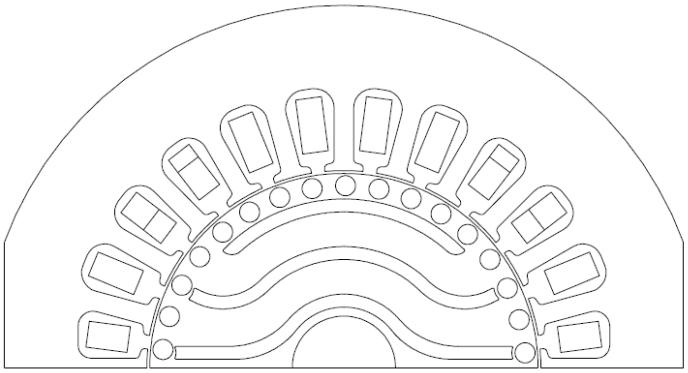

Figure 2.4: Structure of LSSynRM based on induction motor presented in [20], [21] and [22].

2.2.1 The asynchronous starting process

While starting process the voltage in rotor bars is induced due to rotating magnetic field created by stator winding and, thus, the rotors currents with angular frequency $\omega_s - \omega_r$ occur in squirrel cage and slip s is defined same as in an induction motor:

$$s = \frac{\omega_s - \omega_r}{\omega_s}, \tag{2.1}$$

where ω_s is electrical synchronous angular frequency and ω_r is the electrical angular frequency of rotor, respectively. The mechanical angular frequency of rotor Ω_{rmech} is defined according to (2.2), where p is the number of pole pairs.

$$\Omega_{rmech} = \frac{\omega_r}{p} \tag{2.2}$$

The anomaly phenomenon occurs in the half-speed range due to the asymmetric rotor. The rotor currents are not able to create a rotating magnetic field due to the asymmetric rotor, the pulsating magnetic field is created instead. This pulsating field consists of two rotating components, one with positive- and one with negative-sequence. The first positive component of the flux rotates with the angular frequency ω_{pc} in the same direction as the rotor and it creates the positive torque. The second negative component of the flux rotates with the angular frequency ω_{nc} in the opposite direction as the rotor and it creates the negative torque. The final torque, which starts the motor, is the sum of these two components. The angular frequency ω_{pc} and ω_{nc} are expressed in equations (2.3) and (2.4). The second component of the flux and the rotating stator magnetic field make the resulting flux pulsate and this can lead to the failure of reaching the synchronous speed because the angular frequency of the rotor stops and continue work at the half of its rated speed (see Fig. 2.5). The possibility of start failure is reduced with

a smaller saliency ratio. This LSSynRM phenomenon is further studied in [3].

$$\omega_{pc} = (1 - s)\omega_s + s\omega_s = \omega_s \tag{2.3}$$

$$\omega_{nc} = (1 - s)\omega_s - s\omega_s = (1 - 2s)\omega_s \tag{2.4}$$

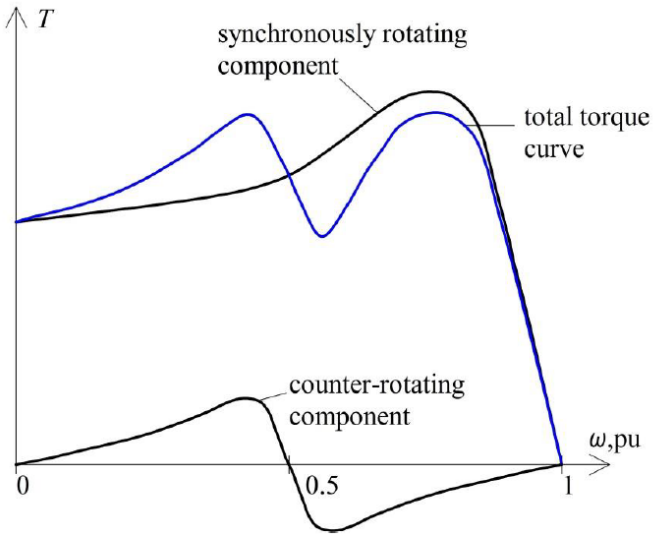

Figure 2.5: Asynchronous torque in half-speed range [3].

2.3 Mathematical description

The mathematical description of LSSynRM is studied in [3], [18], [23] and [4]. The dq-coordinate system is usually used for the description of a synchronous machine because it leads to the compact equations for the motor mathematical description [24]. The Park's transformation is used for transformation of the reference frame of tree-phase in a direct-quadrature-zero (dq0) reference frame. The Park's transformation in matrix form can be applied to any three-phase quantities (e. g. voltages, currents, flux linkages, etc.).

The equation of Park's transformation is defined below:

$$\begin{bmatrix} x_d \\ x_q \end{bmatrix} = C \begin{bmatrix} x_a \\ x_b \\ x_c \end{bmatrix}, \tag{2.5}$$

where C is:

$$C = \frac{2}{3} \begin{bmatrix} cos(\theta) & cos(\theta - \frac{2}{3}\pi) & cos(\theta + \frac{2}{3}\pi) \\ sin(\theta) & sin(\theta - \frac{2}{3}\pi) & sin(\theta + \frac{2}{3}\pi) \end{bmatrix}, \tag{2.6}$$

where position angle θ is defined in Fig. 2.6 and it represents angle between stationary phase a and rotating d-axis. And also:

$$\omega_r = \frac{d\theta}{dt} = p\Omega_{rmech} \tag{2.7}$$

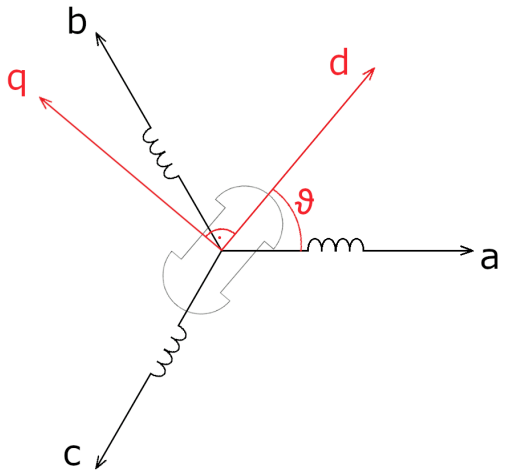

Figure 2.6: The d-q axis reference.

Although the transformation has various forms and coefficients in the literature, the main goal of transformation is to project the three-phase reference frame into dq-axis. The d-q axis is coupled with the rotor because the variable magnetic reluctance is created due to the asymmetric rotor. The d-q reference frame, synchronous to the rotor, is defined in Fig. 2.6. Moreover, the inductances do not depend on the position of the rotor, thanks to the reference frame aligned with the rotor.

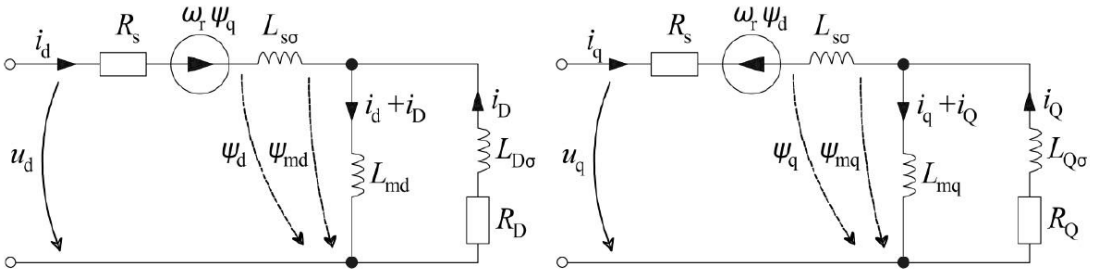

Figure 2.7: Equivalent circuit of LSSynRM in dq-coordinate system [3].

The electrical equations which describe LSSynRM are given below.

$$u_d = R_s i_d + \frac{d\Psi_d}{dt} - \omega_r \Psi_q \tag{2.8}$$

$$u_q = R_s i_q + \frac{d\Psi_q}{dt} + \omega_r \Psi_d \tag{2.9}$$

Squirrel cage is described by the following equations:

$$0 = R_D i_D + \frac{d\Psi_D}{dt} \tag{2.10}$$

$$0 = R_Q i_Q + \frac{d\Psi_Q}{dt} \tag{2.11}$$

Flux linkage equations are:

$$\Psi_d = L_{s\sigma} i_d + \Psi_{md} = L_{s\sigma} i_d + L_{md}(i_d + i_D) \tag{2.12}$$

$$\Psi_q = L_{s\sigma} i_q + \Psi_{mq} = L_{s\sigma} i_q + L_{md}(i_q + i_Q) \tag{2.13}$$

$$\Psi_D = L_{D\sigma} i_D + \Psi_{md} = L_{D\sigma} i_D + L_{md}(i_d + i_D) \tag{2.14}$$

$$\Psi_Q = L_{Q\sigma} i_Q + \Psi_{mq} = L_{Q\sigma} i_Q + L_{mq}(i_q + i_Q) \tag{2.15}$$

$$\Psi_{md} = L_{md}(i_d + i_D) \tag{2.16}$$

$$\Psi_{mq} = L_{mq}(i_q + i_Q) \tag{2.17}$$

The mechanical equation is:

$$T_{em} - T_{load} = \frac{J_{tot}}{p} \frac{d\omega_r}{dt} \tag{2.18}$$

The electromagnetic torque:

$$\begin{aligned} T_{em} &= \frac{3}{2} p(\Psi_{md} i_q - \Psi_{mq} i_d) = \\ &= \frac{3}{2} p((L_{md}(i_d + i_D))i_q - ((L_{mq}(i_q + i_Q))i_d) = \\ &= \frac{3}{2} p(i_q i_d L_{md} + i_q i_D L_{md} - i_q i_d L_{mq} - i_d i_Q L_{mq}) = \\ &= \frac{3}{2} p(i_q i_d (L_{md} - L_{mq}) + i_q i_D L_{md} - i_d i_Q L_{mq}) = \\ &= T_{rel} + T_{cage} \end{aligned} \tag{2.19}$$

Equation (2.19) reports that the electromagnetic torque includes the synchronous component T_{rel} and the asynchronous component T_{cage}. The asynchronous component comes from the squirrel cage currents and is also called "pull-up" torque [4], [18]. T_{cage} depends on the rotor slip s. T_{cage} is present only out of synchronism, whereas T_{rel} always exist. T_{rel} is present due to rotor saliency ratio. The load torque limit of LSSynRM is called pull-out torque and defines maximum load torque for not fall-out of synchronism.

2.4 Pull-in torque

The maximum load torque under which the motor puts given mass of inertia into the synchronism is the pull-in torque. The pull-in torque is higher with the reduced value of the load mass of inertia. The paper [4] investigates possibilities for maximization and improvements of the pull-in capability. There are two main recommendations:

1. Maximization of the saliency ratio is crucial for the performance at synchronous speed.

2. Pull-in torque is improved by reducing the d- and q- axis rotor resistance.

The reducing of the d- and q- axis rotor resistance produces a better pull-up torque. The full filling barriers with aluminium is recommended in [4] as the best way to reach lower q rotor resistance. Also, the higher saliency ratio provides better performance, such as higher pull-out torque, a better power factor and higher efficiency.

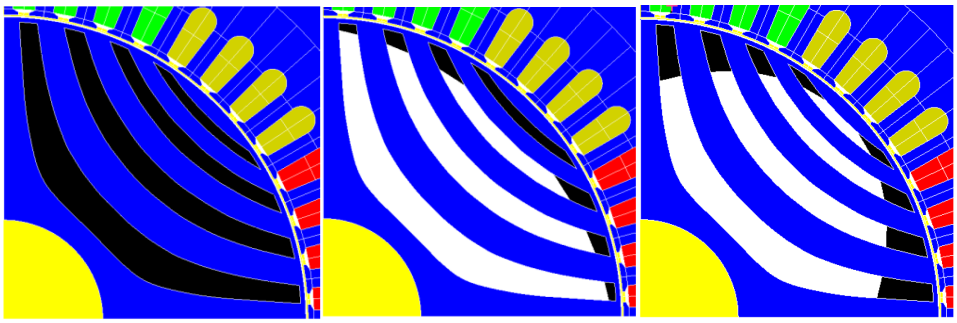

(a) Fully filled flux barriers. **(b)** Elliptical variation 1. **(c)** Elliptical variation 2.

Figure 2.8: The selected topologies of geometries presented in [3].

2.5 Current solutions

The LSSynRM is investigated in literature as the possible replacement for the induction machines. The [3] deals with the LSSynRM with rated output power 30 kW and with the comparison of IM and LSSynRM. The main conclusion within this thesis was that the LSSynRM can compete with IM and have also higher efficiency. Then the starting capability was investigated for eight different geometries. Three of these geometries can be seen in Fig. 2.8. The geometry with fully filled flux barriers, which is shown in Fig. 2.8a, had the best starting capability of presented geometries.

Following paper [25] also deals with starting capability of six different rotors. The selected geometries of this paper are shown in Fig. 2.9. Except the geometry B (see Fig. 2.9b) all geometries reach the synchronous speed and they have efficiency at least 95.0 %. The paper [26] analyse the dependency of the performance on the number of flux

barriers in the LSSynRM. The last chapter deals with comparison of LSSynRM, which is designed by TO within this master thesis, with the prototypes shown in the paper [4].

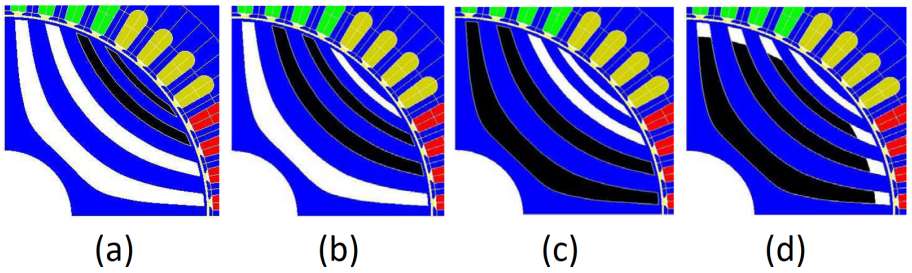

Figure 2.9: Cross-sections of geometries of 4-pole 30 kW LSSynRMs [25].

The single-phase LSSynRMs with two poles were investigated in papers [20], [21] and [22]. The geometry is based on the topology of an induction motor as it can be seen in Fig. 2.10. The patent [27] is proof that the LSSynRMs are investigated not only in the scientific field but also in the industrial field. The topology of LSSynRM based on an induction machine presented in the patent is shown in Fig. 2.11.

Figure 2.10: Topology of 2-pole 2.2 kW LSSynRM [20].

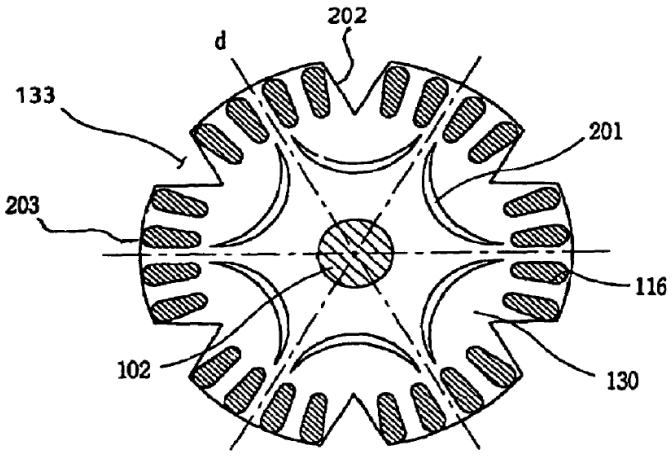

Figure 2.11: Topology of the LSSynRM presented in patent [27].

3 The characterizing the investigated design space

3.1 The optimized motor and its investigated design space

The line-start synchronous reluctance motor is optimized within this thesis. This motor is based on an induction motor and it is very similar to an IM. It has identical stator as the induction motor and, only, the rotor is changed so the synchronous speed can be achieved. The motor has four poles and it's rated power is supposed to be 2200 W. Table 3.1 reports the specification of the optimized motor.

Table 3.1: Specification of the optimized motor.

Parameter	Unit	Value
Number of phases	-	3
Number of poles	-	4
Rated power	kW	2.2
Rated speed	rpm	1500
Rated line-to-line voltage	V	400

The model of LSSynRM for topology optimization purpose is created in Ansys Maxwell and it is shown in Fig. 3.1a. The rotor is divided into small elements in the following form. The number of elements in a radial way is 35 and the number of elements in a spherical way is 90 per pole. In this case, one pole is one-quarter of the rotor. The final number of elements in the designed area is 3150. The numbers of elements in the radial and the spherical way are arranged so the elements on the outer area of the rotor would be the shape of a square. Nevertheless, elements become more rectangular shape in the inner area of the rotor (see Fig. 3.1b). Although better optimization of the rotor can be achieved with the smaller elements, the number of these elements must remain reasonably small due to demanded computational power.

In [16] 7740 elements were used for multi-material topology optimization of interior permanent magnet synchronous motor with the approximately twice smaller rotor compared to the one investigated within this master thesis and the Intel Xeon CPU (2.1 GHz, 12 cores) performed the optimization. In [15] 2256 elements were used for topology optimization of SynRM with the approximately twice smaller rotor compared to the one investigated within this master thesis.

Two states of material can be assigned independently to each element. The line-start synchronous reluctance motor with full barriers filling is optimized in this thesis. The two materials are iron or aluminium. Iron is M470-50A. It is the same material which is used for stator. Aluminium is cast aluminium with conductivity 37,7 MS/m at 20 °C.

The designed area composes from 3150 elements and every each of them can have

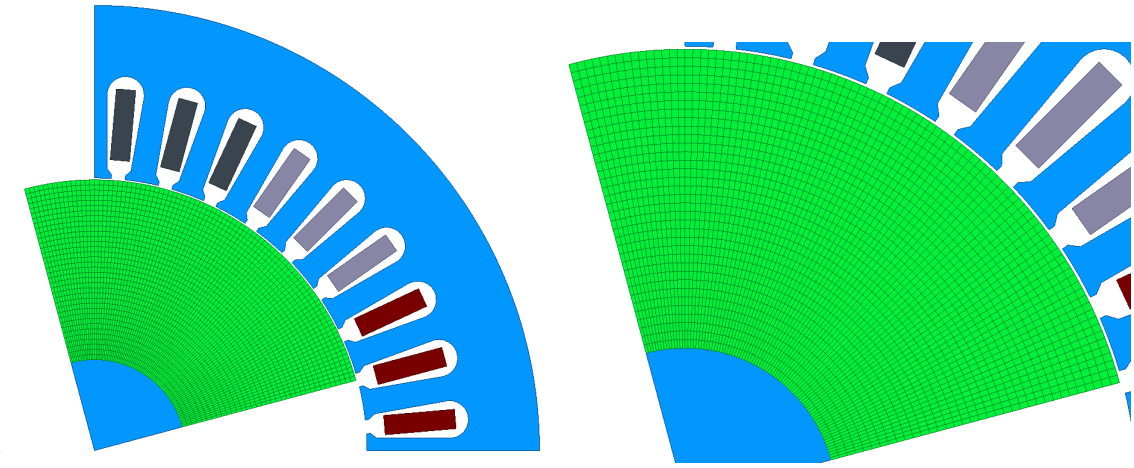

(a) The model of LSSynRM. **(b)** Zoom to designed area (green).

Figure 3.1: The created model in Ansys Maxwell for topology optimization.

two states. In the situation of a simple ON/OFF method for each element that gives 3150^2 possible outcome geometries and the number of parameters is 3150 in such optimization. So other than direct characterizing of design space is necessary, because the number of the variables which are optimized during the optimization, which is performed within this thesis, must be much smaller due to the demanded computational power and DECMO algorithm, that is used in SyMSpace software as an algorithm for the optimization. Thus, the normalized Gaussian network is used for the extreme reduction of the optimized parameters.

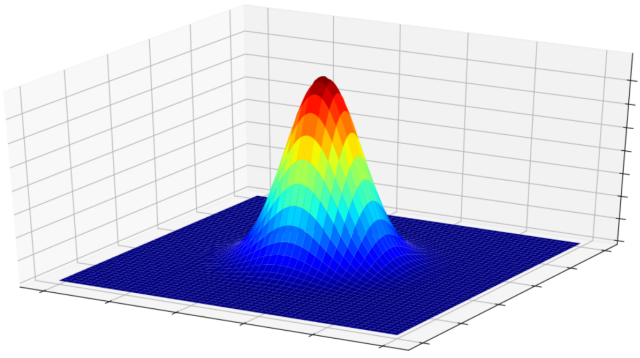

Figure 3.2: The normalized Gaussian function $G(x, y)$.

3.2 The normalized Gaussian network (NGnet)

A Gaussian function is used for defining the normalized Gaussian network. The form of normalized Gaussian function is:

$$g(x) = \frac{1}{\sigma\sqrt{2\pi}} e^{-\frac{1}{2}\left(\frac{x-\mu}{\sigma}\right)^2}, \tag{3.1}$$

where μ is expected value and σ is variance of the normalized Gaussian function, respectively. The form of two dimensional normalized Gaussian function is plot in Fig. 3.2 and is described:

$$G(x,y) = \frac{1}{\sigma_x \sigma_y 2\pi} e^{-\frac{1}{2}\left(\left(\frac{x-\mu_x}{\sigma_x}\right)^2 + \left(\frac{y-\mu_y}{\sigma_y}\right)^2\right)}, \tag{3.2}$$

The normalized Gaussian network is used for optimization of SynRM. The function f(x,y) of the NGnet is given by:

$$f(x,y) = \sum_{i=1}^{N} w_i b_i(x,y), \tag{3.3}$$

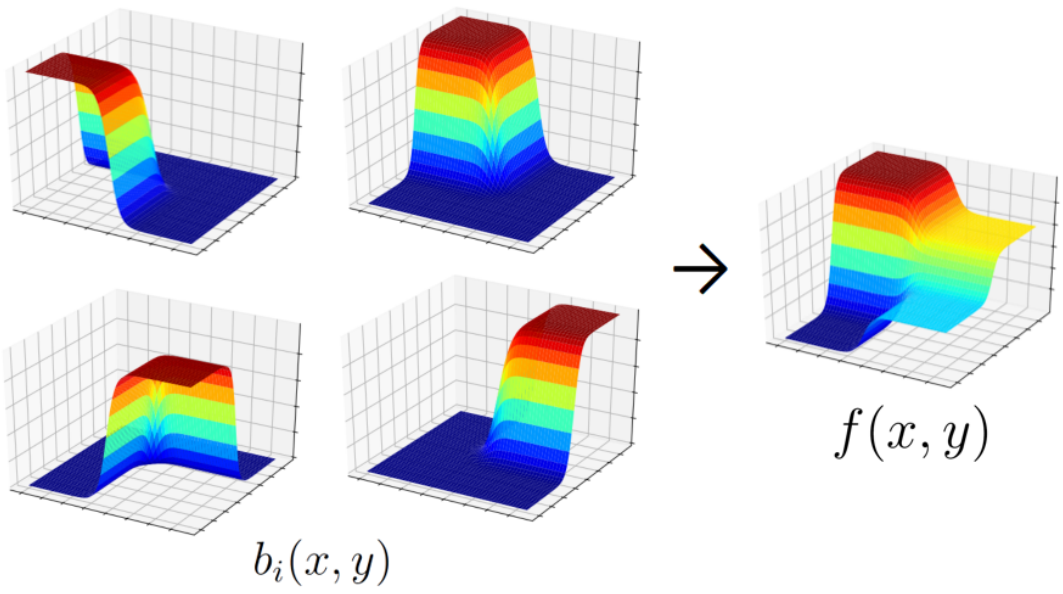

Figure 3.3: The normalized Gaussian network $f(x,y)$.

where w_i and N are weighting coefficient and the number of Gaussian functions, respectively. The portion of one Gaussian function on a position $G_i(x,y)$ and sum of all

Gaussian functions is defined as b_i in equation (3.4).

$$b_i(x,y) = \frac{G_i(x,y)}{\sum_{j=1}^{N} G_j(x,y)}, \tag{3.4}$$

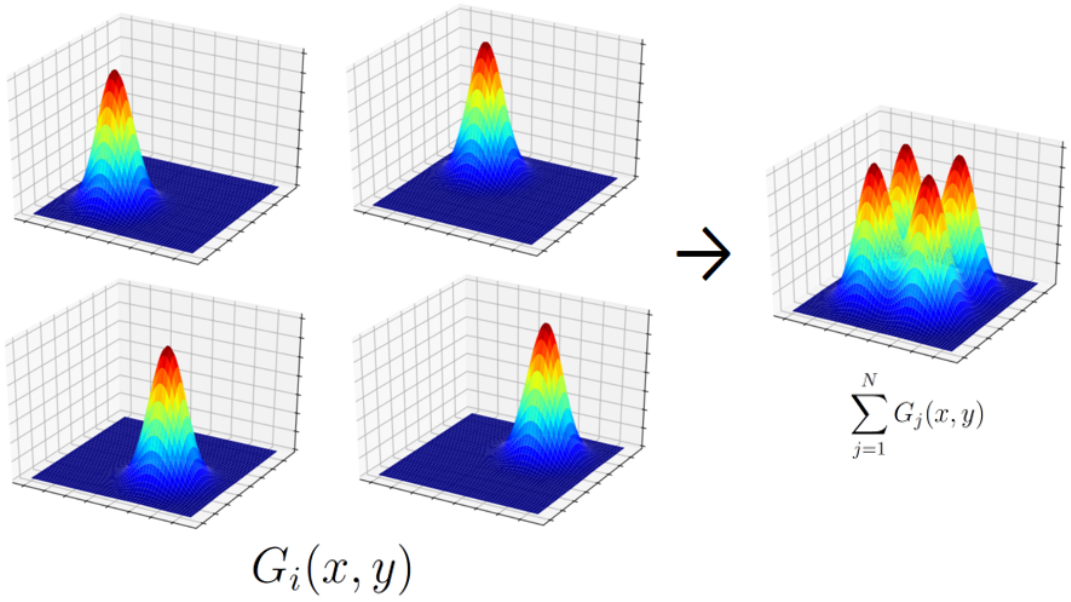

Figure 3.4: The Gaussian functions and their sum.

Each Gaussian function G_i and their sum is shown in Figure 3.4. The Gaussian functions interact with each other. The amount of the interaction defines smoothness of the b_i (see Fig. 3.3) and the final weighted sum of all the b_i functions, thus, the final normalized Gaussian network (NGnet), is also shown in Fig. 3.3.

Each element can be defined by the normalized Gaussian network in the optimized area in the LSSynRM. Each element can be assigned with the defined material properties, e. g. electrical steel or aluminium. Accordingly there are two states $S(x_e, y_e)$ which element can have. $S(x_e, y_e)$ is equal to 0 if the element is assigned with the electrical steel and $S(x_e, y_e)$ is equal to 1 if the element is assigned with the aluminium. $S(x_e, y_e)$ is determined from the output of the normalized Gaussian network $f(x_e, y_e)$ as follows:

$$S(x_e, y_e) = \begin{cases} 0 & \text{if } f(x_e, y_e) \geq 0.5 \\ 1 & \text{if } f(x_e, y_e) < 0.5 \end{cases} \tag{3.5}$$

where x_e and y_e are the coordinates of the centres of each element. The normalized Gaussian function gives a number between 0 and 1. The creation of the normalized Gaussian network, which defines the designed area (see Fig. 3.5), is described in the next chapter.

3.3 Deployment of Gaussian functions in NGnet

The weighting coefficient w_i is an optimized parameter during optimization. The weighting coefficient w_i is a matrix of numbers between 0 and 1 and it modifies the final normalized Gaussian network. The matrix of weighting coefficient w_i is as big as the number of Gaussian functions which are used in the optimization. Thus, the number of deployed Gaussian functions in a designed area is also a number of optimized parameters in the optimization. It was settled that the number of optimized parameters can not be bigger than 45 due to the required computational power and time of the optimization. Also, DECMO algorithm, which is used in SyMSpace for this optimization, was usually used for a smaller number of optimized parameter.

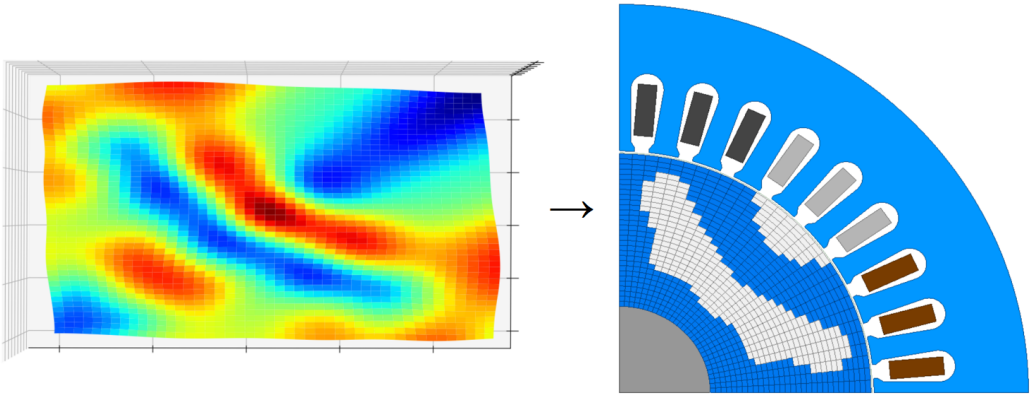

Figure 3.5: The normalized Gaussian network defines final geometry.

Using of NGnet for defining states of elements $S(x_e, y_e)$ is used for possibility define the states of elements $S(x_e, y_e)$ with a small number of optimized parameter and obtain more various resultant geometries obtained by the small number of optimized parameters. The following subchapters deal with the creation of the normalized Gaussian network depending on the deployment of Gaussian functions and variance σ and overleap Ω of the Gaussian functions.

3.3.1 First version of distribution of Gaussian functions

The number of Gaussians in radial way N_{rad} and the number of peripheral Gaussians per pole N_{phr} are set for the first version of distribution of Gaussian function (see Fig. 3.6a). The outer diameter of boundaries for Gaussian functions, thus, the outer diameter of optimized space, is set slightly bigger than the outer diameter of the designed space (the outer diameter of the rotor). The inner diameter of boundaries for Gaussian functions is set slightly smaller than the inner diameter of the rotor and thus the inner diameter of designed space (see Fig. 3.7a). Wider boundaries for Gaussians are chosen because

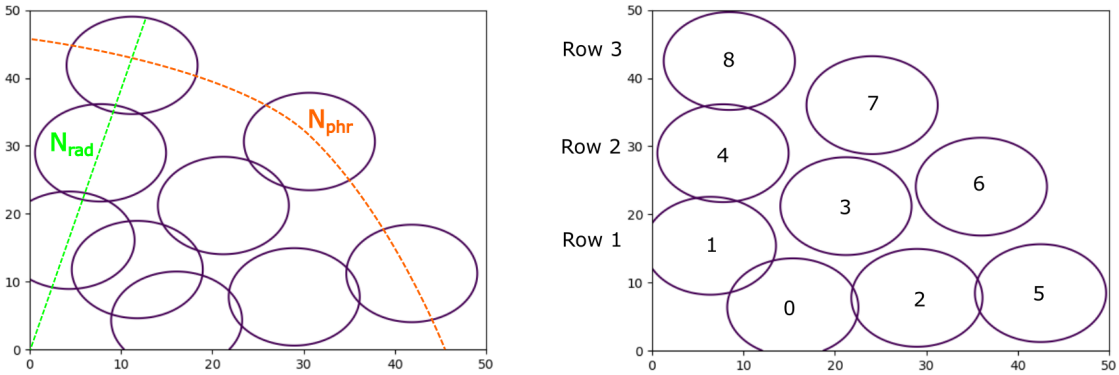

(a) The first version. **(b)** The second version.

Figure 3.6: The deployment of (9) Gaussian functions.

of the satisfying variability of results geometries even in designed areas near to inner and outer diameter of the rotor.

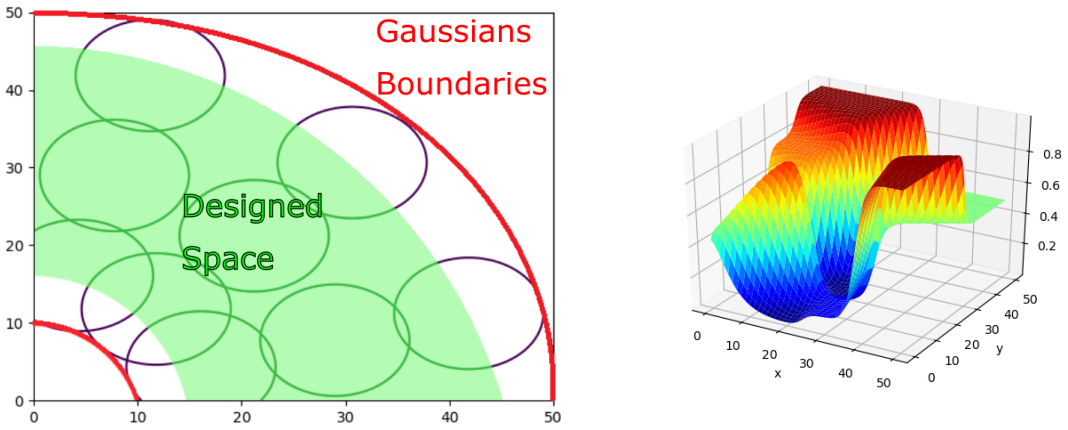

(a) The distribution of Gaussians. **(b)** The normalized Gaussian network.

Figure 3.7: First distribution of Gaussian functions.

The coordinates of the centre of each Gaussians function are μ_x and μ_y. The coordinates are equally deployed in a radial way, but this approach has a problem with an equal distribution in a peripheral way. Fig. 3.7a shows the distribution of Gaussians. The circles represent polylines of the value of 0.5 of each Gaussian function. The Gaussians located near to the shaft have bigger overleap than the Gaussians near to the stator as it is shown in Fig. 3.7a. Although, the final NGnet showed in Fig. 3.7b depends on the weighting coefficients of each Gaussian function, weighting coefficients have not equal impact on the value of NGnet due to the different distribution and the interaction of Gaussian functions in the inner and outer area of the rotor. Therefore, the weighting coefficient of Gaussian function in the inner area of the rotor changes smaller area then the weighting coeffi-

cient of Gaussian function in the outer area of the rotor. Also, the final value of NGnet in the small inner area of the rotor depends on weighting coefficients which are near this area. Thus, this final geometry in this small inner area of the rotor is changed by more than one weighting coefficients and it can be confusing for an optimizing algorithm. The optimizing algorithm should ideally know how and where precisely one weighting coefficient affects the final geometry. The distribution of Gaussian function must be more equal in every direction, because of the described problems.

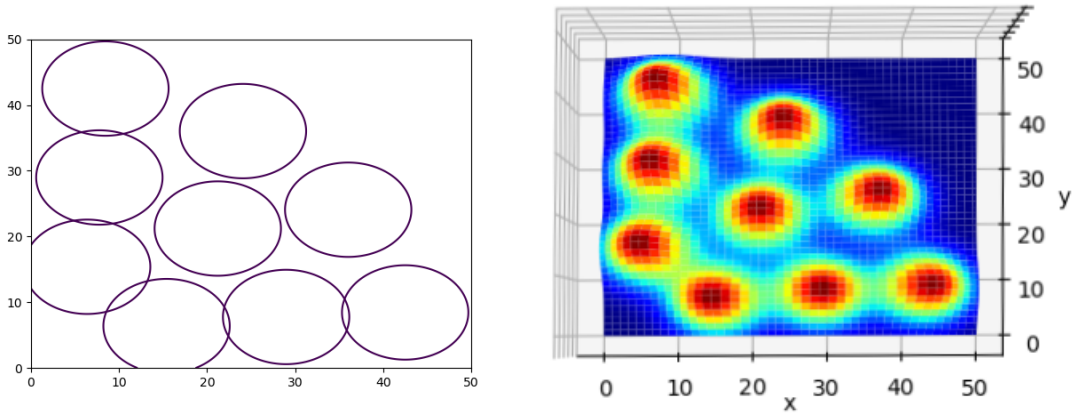

(a) The distribution of Gaussians.

(b) Sum of Gaussians.

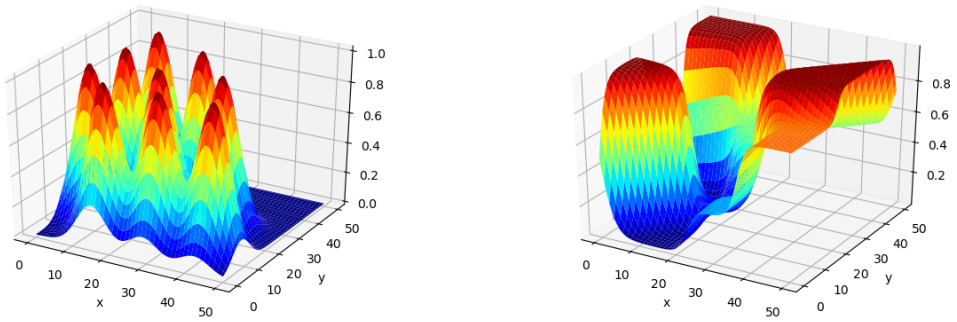

(c) Sum of Gaussians.

(d) The normalized Gaussian network.

Figure 3.8: Second distribution of Gaussian functions.

3.3.2 Second version of distribution of Gaussian functions

The coordinates of the centre of each Gaussian function μ_x and μ_y depend on variance σ, overleap Ω and the inner and the outer diameter of boundaries for Gaussian functions. Variance σ sets diameters of Gaussian functions and overleap Ω sets distances of centres of Gaussian functions as it is shown in Figure 3.9. Firstly, the number of Gaussian functions in a radial way is set, because it is equal in the whole designed area. Then,

the number of Gaussian functions in each row is set depending on the variance and the overleap. Next step of the algorithm is to compute the position of the coordinates of the centre of each Gaussian function μ_x and μ_y. The rows and the numbering of Gaussian functions are shown in Fig. 3.6b. The numbering of Gaussian functions is important because it is later used for the weighting coefficients in the same order.

Fig. 3.6b shows the difference between the first and the second version of the distribution of the Gaussian functions. It is obvious, that the second version of the distribution of Gaussians is greatly more beneficial for the optimization than the first one.

The second version of the deployment of the Gaussian functions in Fig. 3.8a is equalized through the whole optimized area. The Gaussian functions located near to the shaft have approximately equal overleap Ω as the Gaussian functions near to the stator as it is shown in Fig. 3.8b and Fig. 3.8c. The final normalized Gaussian network showed in Fig. 3.8d depends on the weighting coefficients of each Gaussian functions. The weighting coefficients have an equivalent impact on the value of the normalized Gaussian network in the whole area of the rotor due to the same distribution and overleap Ω of Gaussian functions in the inner and the outer area of the rotor in case of this second distribution.

3.3.3 Variance and overleap

The second version of the deployment of the Gaussian functions, which is equalized through the whole optimized area, allows analysis of dependency of the final normalized Gaussian network on variance σ and overleap Ω. The difference between two different sets σ and Ω is shown in Figure 3.9. Values of σ and Ω and the final number of Gaussian functions for such values are shown in Table 3.2. The variance σ and overleap Ω are set so the final numbers of Gaussian functions stationed in the designed space are comparable. Also, the final setting of variance σ and overleap Ω is in the lowest row of Table 3.2. The identical weighting coefficients are used for both NGnets in Fig. 3.9c and Fig. 3.9d. Accordingly, the final NGnets are very similar and they differ only in smoothness. The smoothness depends more on overleap Ω than on variance σ.

Table 3.2: Settings of variance and overleap.

Variance σ	Overleap Ω	Number of Gaussian functions N
2.5	0.2	41
1.0	-1.0	42
2.0	0.3	40

The diversity of final NGnet, and thus the final geometry, depends on the number of Gaussian functions which is set by variance σ and overleap Ω. The number of Gaussian functions is larger with the smaller variance σ and with larger overleap Ω. The

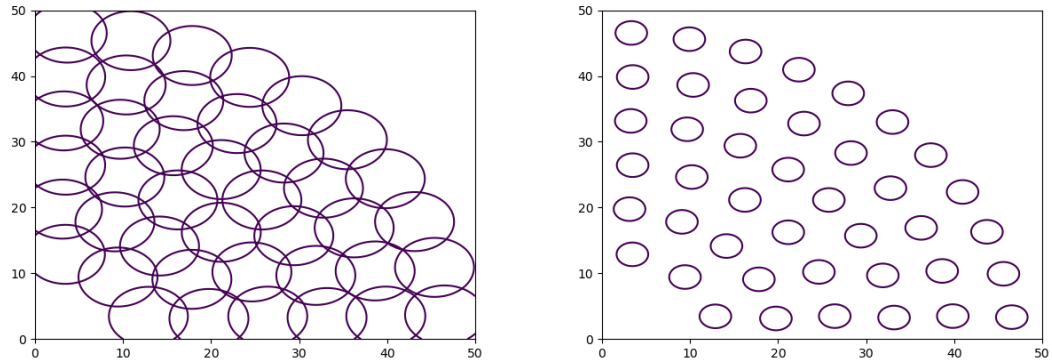

(a) The distribution of Gaussians $\sigma = 2.5; \Omega = 0.2$. **(b)** The distribution of Gaussians $\sigma = 1.0; \Omega = -1.0$.

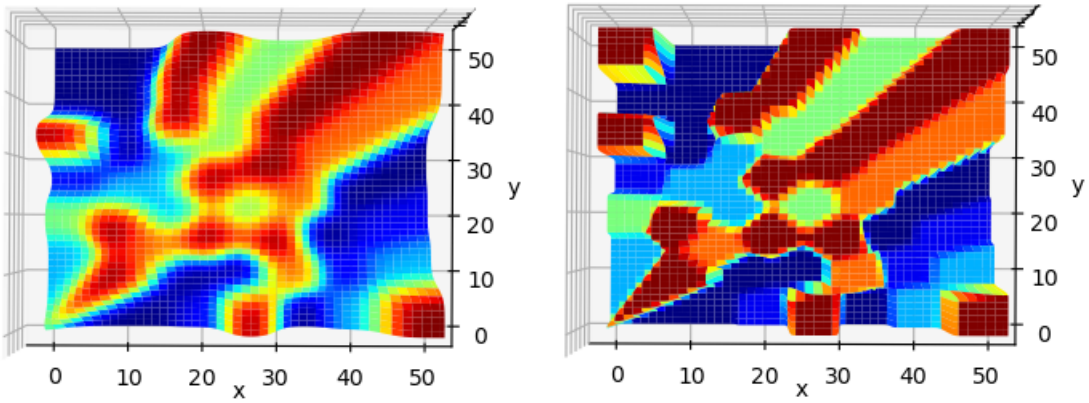

(c) NGnet $\sigma = 2.5; \Omega = 0.2$.

(d) NGnet $\sigma = 1.0; \Omega = -1.0$.

Figure 3.9: Deployment dependency on variance σ and overleap Ω.

smoothness of NGnet is desirable because then there are not present any "detached particles". The term "detached particles" is explained later.

Also, three different distributions of the Gaussian functions are investigated in paper [16]. The three different distributions are shown in Fig. 3.10a. The dependency of fitness of final geometry vs the number of generations is analysed in NGnet-MTO. The results of changes in average fitness during the optimization process are shown in Fig. 3.10b. The distribution (C) with small variance σ has the worst fitness. It is caused by small smoothness of final NGnet and the low representation ability. The small variance σ and small overleap Ω leads to uncomplicated geometries.

The fitness of the deployed Gaussian functions (A) and (B) is quite comparable. And fitness of (B) achieved better results in less number of the generations before the first step. The steps in Fig. 3.10b are caused by a performing of heuristic local search (LS) after each 20^{th} generations of a genetic algorithm (GA). After the first LS, the fitness of distribution (A) and (B) are almost equal. Using of LS combined with GA improves very

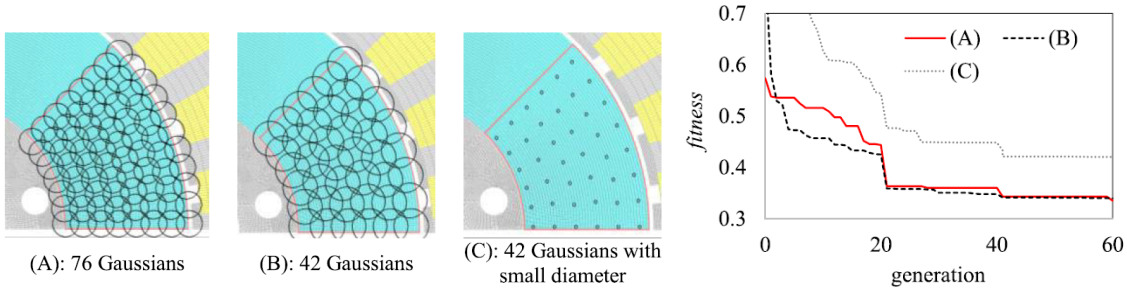

(a) Deployed Gaussians used in optimization [16].

(b) Changes in average fitness during optimization process [16].

Figure 3.10: Comparison of the different Gaussians distributions in paper [16].

effectively the topology optimization when a large number of the Gaussian functions is used in the optimization. Nevertheless, the final geometry with the best result is the one, where the distribution (A) was used during optimization. The disadvantage of the distribution (A) is a long size of chromosome in GA (a big number of Gaussian functions), that leads to longer time to achieve a satisfying fitness without LS. On the other hand, the distribution (A) has great representation ability and it gives smooth shapes of final geometries.

The resultant rotor shapes for three distribution (A), (B) and (C) is shown in Fig. 1.6. Although the distributions of Gaussian functions in Fig. 3.10 are used for approximately twice smaller rotor than it is optimized within this master thesis, a similar number of Gaussian functions in distribution (B) is used for topology optimization in this thesis. It probably results in more simplified geometries than it could be achieved with more Gaussian functions in twice bigger space. Still, the representation ability remains the same as in [16] and the shape of final geometry should be smoother concerning the size of the rotor.

3.3.4 Final version of distribution of Gaussian functions

The final number of the optimized parameters, thus the number of Gaussian functions used in NGnet, is set to 40. Although the distribution shown in Fig. 3.11b has the quite satisfying representation ability, another improvement in the distribution is made. On the one hand, the rotor could be asymmetrical with NGnet shown in Fig. 3.11d and it could possibly bring many unusual shapes of the final geometries. On the other hand, the line-start synchronous reluctance motor is optimized within this master thesis. The same sequence of phases can not be always guaranteed as the motor is directed on line. Thus, the direction of rotor movement is not always the same, so the symmetrical rotor is chosen. In advance, the symmetrical rotor brings the possibility of an increasing number of Gaussian functions used in the optimization. In fact, the number of optimized

parameters remains the same, but the representation ability is better due to the different distribution of the Gaussian functions which is shown in Fig. 3.11a.

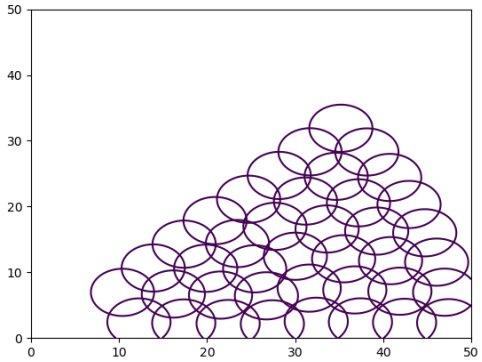

(a) The final distribution of Gaussians.

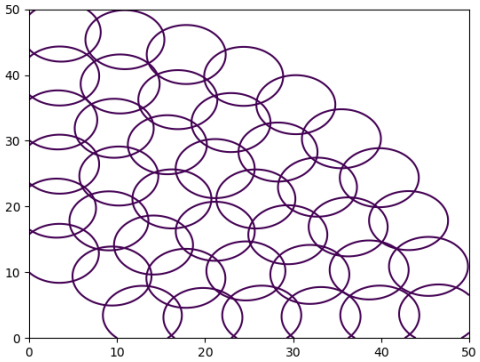

(b) The distribution of Gaussians in the whole designed area.

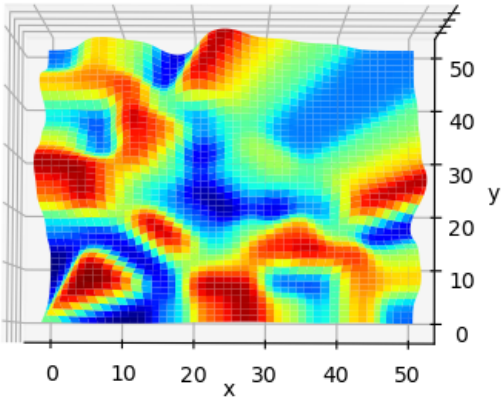

(c) The symmetrical NGnet.

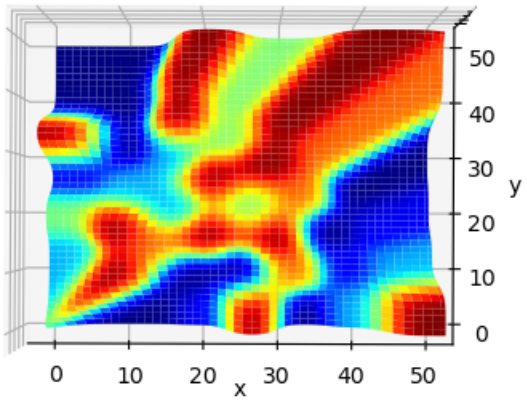

(d) The asymmetrical NGnet.

Figure 3.11: The comparison of symmetrical (a) (c) and asymmetrical NGnet (b) (d).

At this moment must be decided how the symmetric NGnet will be created. Using 80 Gaussian functions with mirroring the equal weighting coefficients is one possibility. The other possibility is chosen within this thesis which is following. NGnet is created in the one half of pole only with using 40 Gaussian functions. Thus, the number of Gaussian functions is 40 and all these Gaussian functions are deployed in one half of one pole (see Fig. 3.11a). Next, the NGnet in the one half of the pole is created as it can be seen in Fig. 3.12a. The previous sentence is not precisely correct, because the function f(x,y) of the NGnet is given by equation (3.3) for all $x, y \in \langle 0; 50 \rangle$. So, the normalized Gaussian network is created for the whole rotor and even for the area out of the rotor (shaft, air, stator), but the only part which is valuable for the optimization is the one half of the rotor where the Gaussian functions are deployed. After that, the function f(x,y) is mirrored

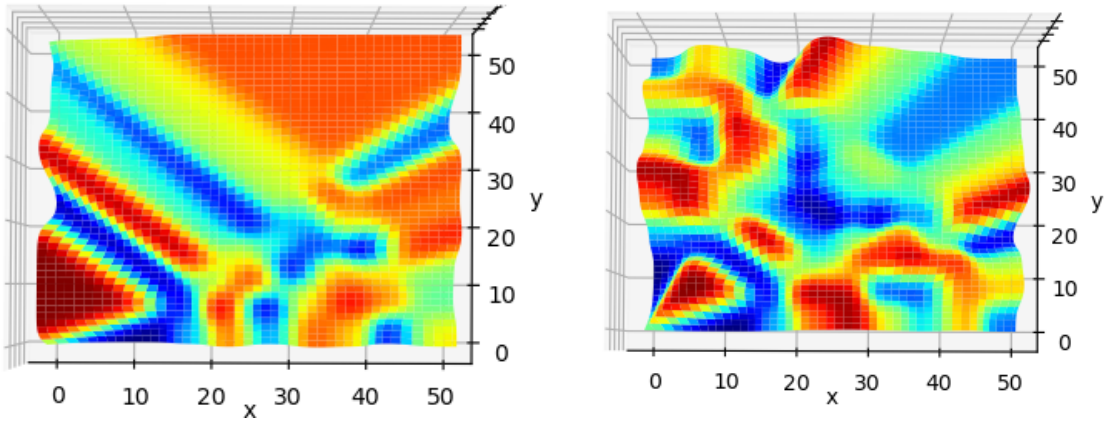

(a) The NGnet created by distribution in Fig. 3.11a.

(b) The symmetrical NGnet.

Figure 3.12: Alternation of asymmetrical NGnet into symmetrical NGnet.

along the function: $x = y$. This creates the final NGnet which is used for the optimization of LSSynRM in this master thesis (see Figure 3.12b).

4 Topology optimization of line-start synchronous reluctance motor

Topology optimization of line-start synchronous reluctance motor is performed in this master thesis and SyMSpace is used for the optimization. SyMSpace is a software tool for system simulation and optimization. The paper [28] SyMSpace presents methods to accelerate the optimization of electrical machines with SyMSpace, especially highly-efficient permanent magnet motors. Therefore, SyMSpace can reduce the development time of electric machines. It is a powerful tool used for optimization thanks to the robust structure and the simple integration of external simulation software. Parameters, which can be simulated automatically, are stored in a tree-like hierarchic structure [28] (see Fig. 4.1). The Optimizer is part of SyMSpace, that performs optimization of the project created in SyMSpace. It contains MOEAs for efficient optimization:

- **NSGA-II** - the non-dominated sorting genetic algorithm II [29], [30].
- **SPEA2** - the strength Pareto evolutionary algorithm [31].
- **DECMO** - differential evolution-based, the coevolutionary multi-objective optimization algorithm [32].

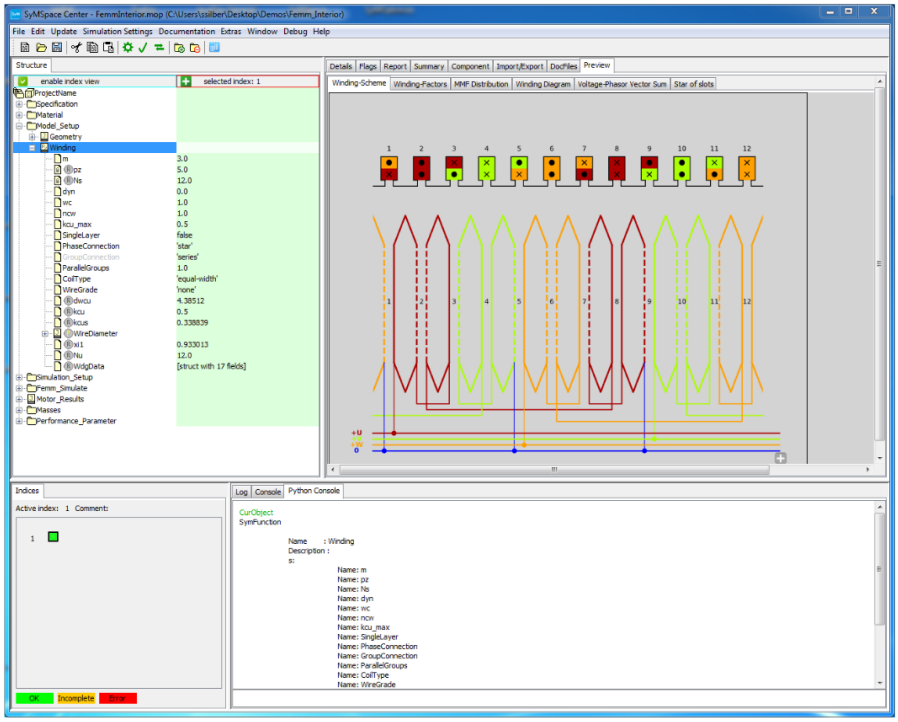

Figure 4.1: Graphical user interface of the simulation framework SyMSpace [28].

Software SyMSpace is used for topology optimization of line-start synchronous reluctance motor. The Ansys Maxwell software tool is chosen for finite element analysis

(FEA). So, the communication between these two software tools needs to be done. The interface to both internal and external simulation modules is established by functions, which are the central elements in SyMSpace. The interface is realized by input and output lists of parameters [28]. The script language Python is used to implement functions in this master thesis.

4.1 SyMSpace project for topology optimization of LSSynRM

The model in Ansys Maxwell is created in the previous chapter. Also, the parameters of the normalized Gaussian network for the optimization are set. The interface and structure of created SyMSpace project for TO of LSSynRM is shown in Figure 4.2. It can be seen that the tree-like structure begins with the main function *GausMxwl*. This function in SyMSpace interface contains:

1. **Three subscripts and fields for their results**
    - Script for topology creation
    - Script for initial analysis
    - Script for transient analysis
2. **Fixed parameters**
    - Parameters of rotor network
    - Parameter of Gaussian function variance σ
3. **Optimized parameters**
    - Weighting coefficients of each Gaussian function
4. **Objectives**
    - EF - Efficiency
    - PF - Power factor
    - TR - Torque ripple
5. **Constraints**
    - EF - Efficiency
    - PF - Power factor
    - TR - Torque ripple
    - C - Speed

The transient analysis must be performed when the LSSynRM is optimized. That is the main problem of topology optimization of LSSynRM. The transient analysis is time-consuming. The transient analysis of one individual, thus one geometry, takes approximately 2-3 hours depending on computational power and finest of mesh. The DECMO algorithm requires at least 20 generations with 100 individuals each to reach a satisfying convergence of the Pareto front [28]. That means that at least 2 000 transient analysis must be performed if there are no other restrictions, but normally even more individuals must be evaluated. Performing such many analysis would take months maybe more for achieving the geometry with satisfactory performance. Thus, the main function in SyMSpace is divided into three more functions to reduce computational time.

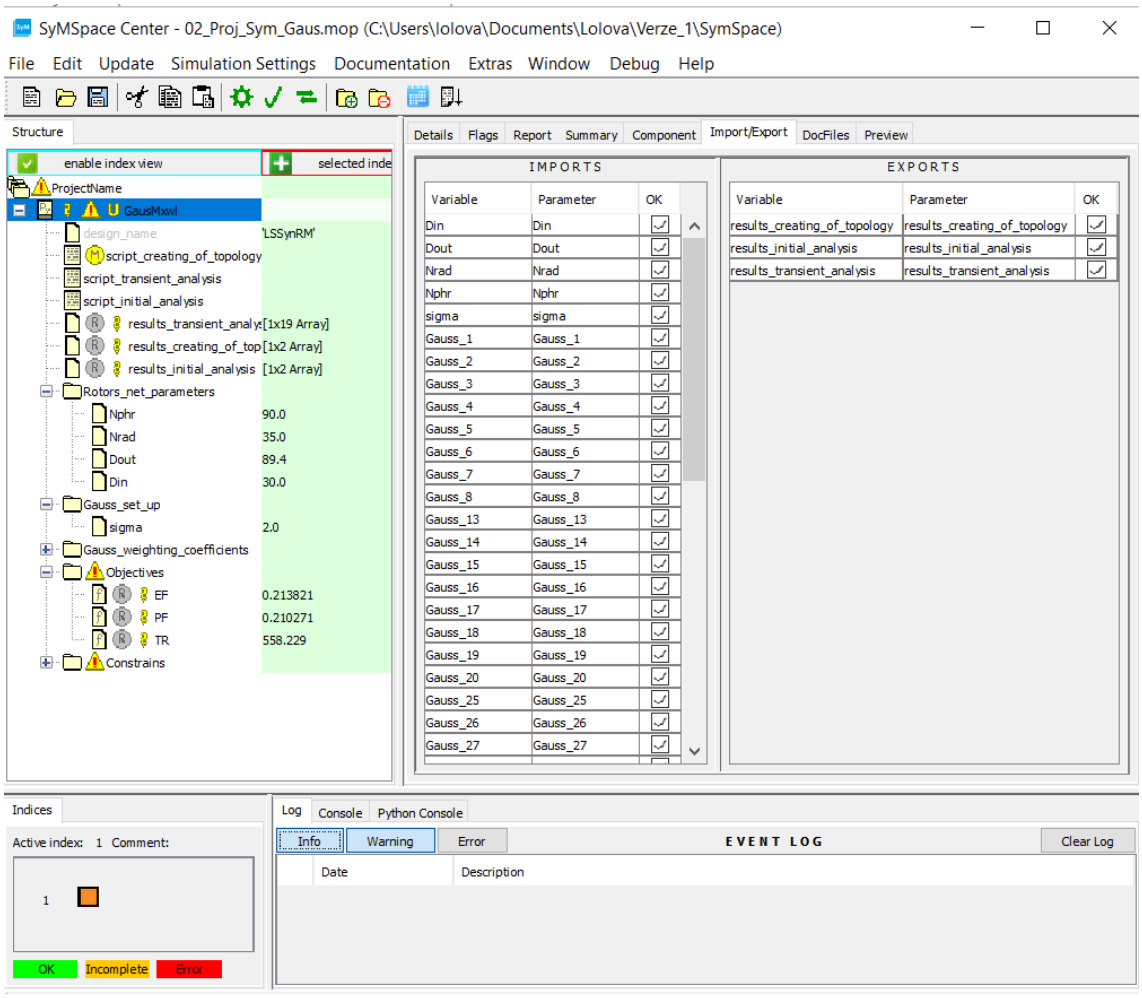

Figure 4.2: Prepared SyMSpace project for topology optimization of LSSynRM

4.2 SyMSpace Optimizer setting

The general setting of the optimized project in SyMSpace Optimizer is described in this chapter. Firstly, the SyMSpace project for optimization is chosen and problem, which is

supposed to be solved, is created. Secondly, the selecting of variables for optimization is done. The setting of parameters for optimization is shown in Table 4.1. It can be seen that the parameters of weighting coefficients are the only parameters chosen for optimization. The constraints for these parameters can be seen also in Table 4.1. The step is set to 0.0 during optimization because it was default setting. On one hand, the weighting coefficients does have values with many decimals places (15) during this optimization, that may lead to more possible geometries. On the other hand, thanks to results of optimization it is clear that the step should be set to a small number, e.g. 0.001 or 0.0001, because the changes smaller than ten-thousandths does not have a substantial impact on the final geometry.

Table 4.1: Optimized parameters setting.

Name	Step	Min	Max
Gauss_0	0.0	0.0	1.0
Gauss_1	0.0	0.0	1.0
...	0.0	0.0	1.0
...	0.0	0.0	1.0
Gauss_39	0.0	0.0	1.0

Constraints and objectives can be seen in Table 4.2. This setting is very important for optimizer because it defines how the results of each individual will be sorted. Objectives are efficiency EF, power factor PF and torque ripple TR. The efficiency and power factor are maximized with constraints from 0.0 to 1.0. The torque ripple is minimized and maximal value can not be bigger than 100.0. The values of torque ripple are in percentages. The final constraint is for speed of the motor, because it is possible that the line-start synchronous reluctance motor can sometimes fail to reach synchronous speed and continue work at half of its rated speed or even there could be a total failure of the starting process. So, the speed at the two last calculated period is controlled and it is accepted only if the speed is between 1400 and 1600 revolutions per minute.

Table 4.2: Objectives and constraints setting.

Name	Objective	Min constraint	Max constraint
EF	MAX	0.0	1.0
PF	MAX	0.0	1.0
TR	MIN	0.0	100.0
Speed, C	NONE	1400.0	1600.0

Pool size is set to 21. Hence, the SyMSpace Optimizer computes 21 parallel individuals. So, the Optimizer creates parameters sets of weighting coefficients and calls

function *GausMxwl* for each of 21 individuals. Then the algorithm of *GausMxwl* function is performed. As soon as one of the 21 individuals is evaluated, the next individual is automatically computed. So, 21 individuals are computed in parallel at any time during the whole optimization. The maximal computational time of one individual, called function timeout, is set to 360 minutes. If the evaluation of one individual takes longer this individual is recognized as an error. Autosave interval is set to 100 individual in case of fatal error or blackout of the server. The solver settings remain in default settings.

4.3 Evaluation algorithm of single individual

This chapter deals with the evaluation algorithm of one individual. It was already mentioned that transient analysis demands a significant computational time. So, the main purpose of the evaluation algorithm is to prevent not promising geometries to be transient analyzed. Moreover, the initiation of communication with Ansys Maxwell is slow. The Ansys Maxwell is a highly robust software for FEA, but it has great demands for computational power. Only the opening of the project and creating of topology based on a Gaussian network takes a lot of time. Therefore this is the other reason why the evaluation algorithm of one individual is divided into three subscripts.

The topology optimization has the potential to create unfeasible geometries. The evaluation algorithm of one individual is shown in Fig. 4.3. It begins with SyMSpace Optimizer which creates Gaussian weighting coefficients set for one individual. Following that the SyMSpace Optimizer call prepared the project in SyMSpace. In this project the main Python function *GausMxwl* is called. The *GausMxwl* imports Gaussian weighting coefficients set and starts to call the first subscript *Topology creation.* Subscript *Topology creation* is also a Python script.

4.3.1 Geometry check

The first subscript *Topology creation* creates the normalized Gaussian network based on the imported Gauss weighting coefficients. At this moment the first restriction to an individual is applied. Aforementioned unfeasible geometries are geometries which contain detached particles. The detached particles can be a confusing term when the rotor with full filled barriers is investigated within this thesis. There are not truly any detached particles as the final rotor is one piece made of aluminium and iron. However, the core of the rotor is made from laminated sheets, because this way the eddy current losses are reduced. Thus, the rotor laminated sheet must be one piece. Therefore, the detached particles are particles of iron which are not connected to any other, or more of these iron particles creates the ”island” in the geometry, which is/are not connected to the shaft. If the detached particles are present in the geometry, the geometry can not be manufactured.

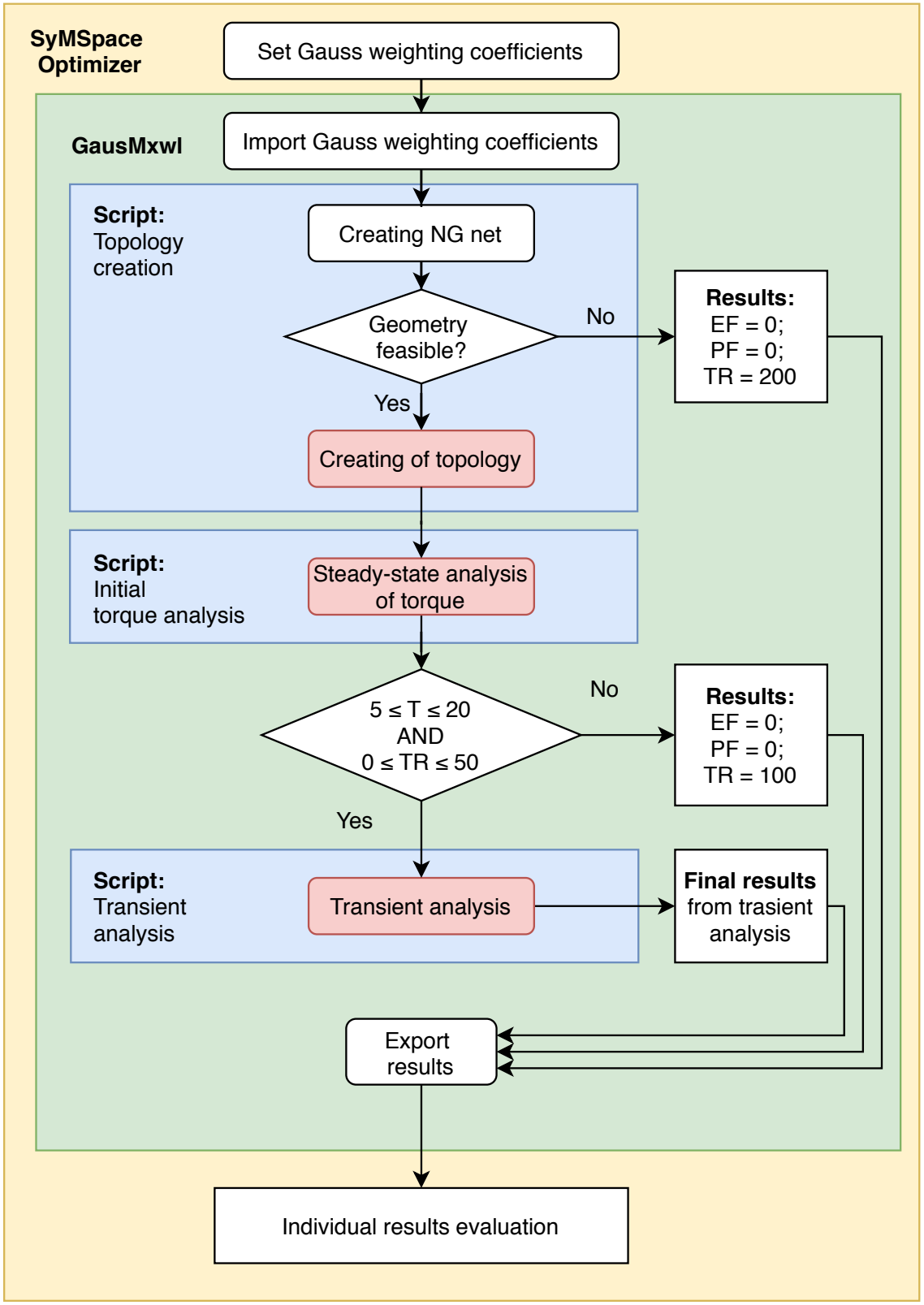

Figure 4.3: Evaluation algorithm of one individual.

The geometry test algorithm is created to prevent these detached particles. As can be seen in Fig. 4.3 the test if the geometry is feasible follows the NGnet creation and it is followed by topology creation. The red blocks present initiation and communication with Ansys Maxwell. So, the geometry test algorithm runs only in Python. If the geometry is evaluated as unfeasible the script *Topology creation* is stoped and it returns results into the main script *GausMxwl*. Next the main script export this results in SyMSpace Optimizer and there the results are evaluated by the running solver, in this case, it is the DECMO algorithm. Thanks to this step the communication with Ansys Maxwell is not even initiated and everything is running only in Python. This part takes approximately 2-4 minutes depending on capacity utilization. Thus it is a remarkable reduction of time. If the geometry test was not involved in optimization algorithm this unfeasible geometry would be transient analysed for 2-3 hours instead of 2-4 minutes.

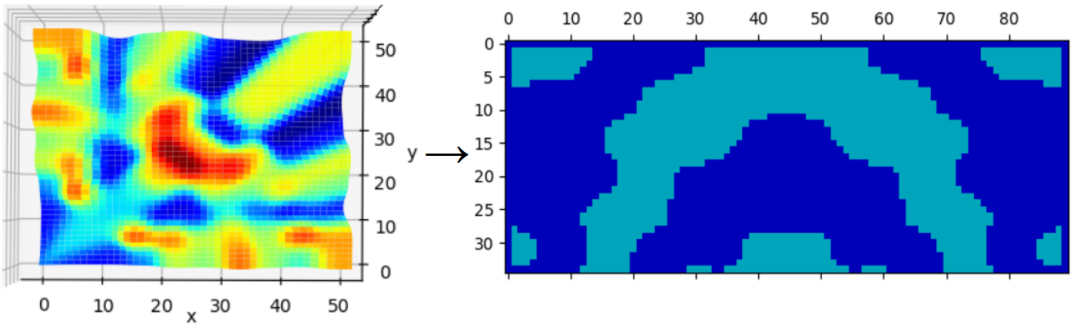

Figure 4.4: NGnet transformation into matrix defining the elements.

The geometry test algorithm starts with the transformation of NGnet into the matrix of 0 and 1 based on equation (3.5). This matrix has dimensions as the number of elements (35 x 90) in the prepared model in Ansys Maxwell. The transformation into the matrix is shown in Fig. 4.4. The dark blue presents the iron and the light blue presents the aluminium. The edges of this matrix are set to iron. This change is shown with a dark yellow colour in Fig. 4.5. The first element with matrix coordinates $[0; 0]$ is chosen as the starting point of the algorithm, also called as the start node. The top row is checked as the iron because it was set as the iron. Then the algorithm moves to the second row to the element $[1; 0]$ and next it continue in the row to the right to the element $[1; 1]$. The only four-way testing algorithm is acceptable in this variation of geometry test because two elements touching at the corners can not be considered connected. So, the element $[1; 1]$ is controlled if it is connected to the checked iron, which in this case are the elements $[1; 0]$ and $[0; 1]$. Thanks to these two elements the element $[1; 1]$ is also check as the connected iron. The color of this element turn green as it is shown in Fig. 4.5a. The elements $[2; 1]$ and $[1; 2]$ are iron, but they are not checked yet. So the connection to them is irrelevant. Next, the algorithm checks all the other elements. This algorithm is very alike as the flood-fill algorithm.

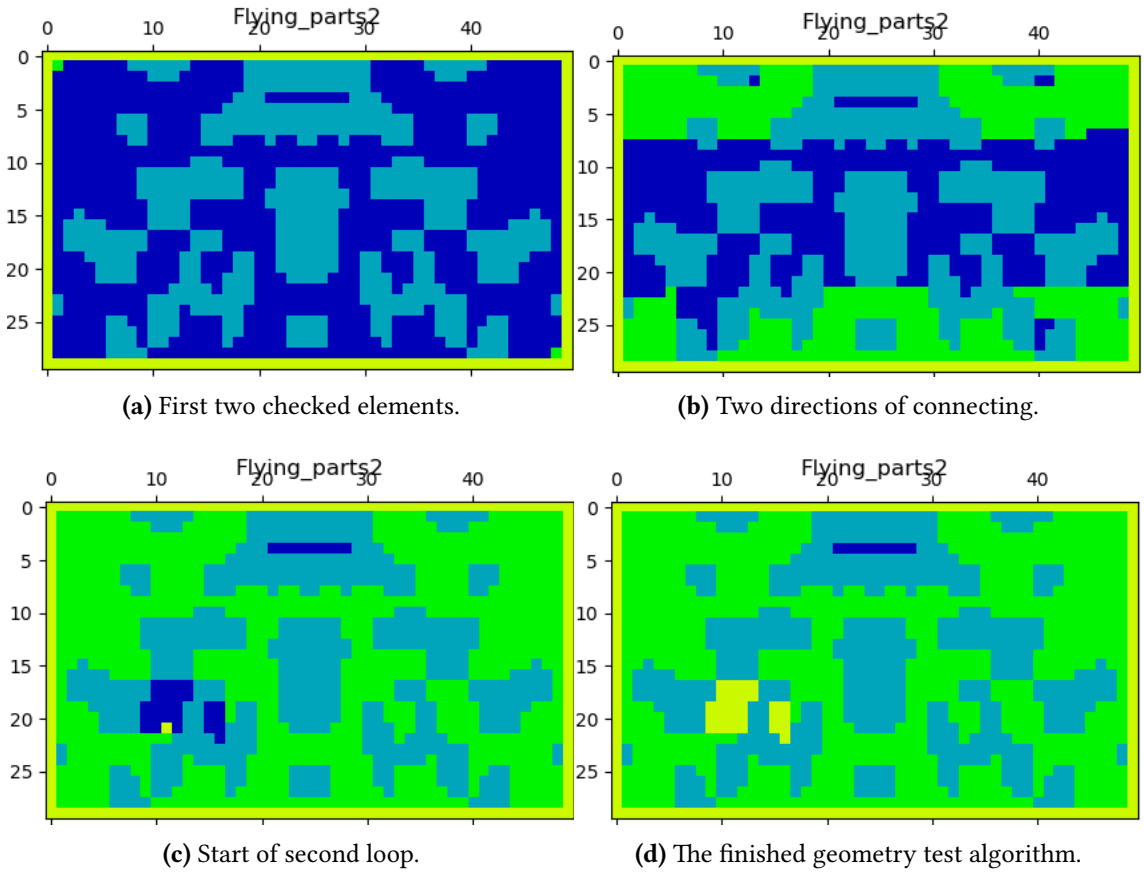

(a) First two checked elements.

(b) Two directions of connecting.

(c) Start of second loop.

(d) The finished geometry test algorithm.

Figure 4.5: The geometry test algorithm.

For the time reduction of geometry test algorithm there is set the other start node, in which case, the check algorithm moves in the opposite direction. This can be seen in Fig. 4.5b. The point of the beginning of the new cycle (bright yellow) is shown in Fig. 4.5c. The result of the geometry test algorithm is shown in Fig. 4.5d. The dark yellow area is the edges sets as the iron. The green and bright yellow areas are the connected iron elements which create with edges one piece. Bright yellow colour only shows that this area where checked in the second loop of the algorithm. The dark blue areas display the iron elements which are not connected to the checked iron. Thus, this area presents this ”island” which would be impossible to be manufactured. So the geometry test algorithm evaluates this geometry as unfeasible and the script *Topology creation* is stopped (see Fig. 4.3).

If the geometry is evaluated as feasible, the script *Topology creation* continues with topology creation in Ansys Maxwell. The communication with Ansys Maxwell is initiated in this step and elements are defined to iron or aluminium based on the geometry tested matrix. The matrix sorting is actually done in Python and the final string of iron elements and string of aluminium elements is sent to the Ansys Maxwell. The ”creation” of topology means that the Python script copies the prepared project with the

prepared model (see Fig. 3.1a) and assigns the elements with the material based on the given strings. The setting of the project is already done in the prepared project, so the algorithm does not have to do that. The new geometry, thus the new file with copied and changed project in Ansys Maxwell, is saved and the first subscript ends.

4.3.2 Torque check

After the first subscript *Topology creation* ends, the main function *GausMxwl* continues with a next step depending on the feasibility of the geometry. If the geometry is feasible and it was successfully created in Ansys Maxwell, the second subscript *Initial torque analysis* starts. The second subscript also saves time, because the steady-state analysis is performed to obtain values of torque in steady-state. The values of torque should be analysed in advance to the long transient analysis. Even if the geometry is evaluated as feasible, it does not mean it is a promising geometry, which gives satisfactory results.

The solving time in this simulation is set to only 4 ms, but it is enough to obtain the average torque and approximate torque ripple. The steady-state analysis takes about 20-30 minutes. Thus, this script once again initiates the communication with Ansys Maxwell and performs the steady-state analysis. After the analysis in Ansys Maxwell is done, the Ansys Maxwell project is saved and closed. The values of torque are export in the second subscript and then in the main function *GausMxwl*. The main function evaluates the values of torque and torque ripple as can be seen in Fig. 3.1a. Depending on results *GausMxwl* calls the final subscript *Transient analysis* or continues a similar way as the first subscript when the geometry is not feasible.

4.3.3 Transient analysis

The third subscript *Transient analysis* is the last subscript. The communication with Ansys Maxwell is initiated. The prepared Ansys Maxwell project is called and the transient analysis is performed. Then the results are exported in the main function *GausMxwl*. It needs to be said that the project in Ansys Maxwell includes two designs. These two designs have equals geometries created in the first script, but the analysis settings are different. First is for initial torque analysis and the second is prepared for transient analysis. The solving time in this simulation is set to 0.35 s with step 0.0002 s. The expected time of transient analysis was 2-3 hours, but some individual still can not fulfil the time-out of 360 minutes. Of course the final evaluation time of one individual is prolonged by the time of these additional tests - geometry test algorithm and initial torque analysis. Thus, the unfeasible and unpromising geometry is analysed for 5-30 minutes only, but the feasible and promising geometry is transient analysed for 2-3 hours plus the time of additional testing (5-30 minutes). The individuals that take more time than 360 minutes to be evaluated are the error ones. Average time of evaluating a single individual is

4-5 hours, but 21 individuals are evaluating parallel at the one moment.

The evaluation of single individual ends with results export from main function *GausMxwl* into SyMSpace Optimizer. Then the solver evaluates the results according to SyMSpace Optimizer setting.

4.4 Results of optimization

The whole performed optimization ran on the two processors: Intel(R) Xeon(R) CPU ES-2660 v3 (2.60 GHz); physical cores: 20; logical processors: 40. The optimization ran for one and half month. The optimization algorithm evaluated approximately 15 000 sets of weighting coefficients. The buffer was set to 4 500 individuals. Thus, the buffer creates 4 500 sets of weighting coefficients which are equally distributed in 40-dimensional space. After evaluation of the initial buffer, the optimization starts. Around 10 individuals went through the evaluation algorithm of a single individual into the transient simulation. It means that 99.98 % of initially created geometries was sorted out by the conditions in the evaluating algorithm of a single individual. The most geometries were restricted due to unfeasible geometry and the others due to low torque. After evaluation of buffer, the solver of SyMSpace optimizer can start the real optimization, but it has only 10 initial geometries. Because of these results, it would be better if the buffer was bigger and more geometries were found before optimization. Still, satisfying results were obtained from optimization. The memory archive of individuals who fulfil the conditions in SyMSpace optimizer is shown in Fig. 4.6. The dark points present the Pareto front of the optimization. Thus, these individuals have the best performance. It shadow points show the convergence of optimization algorithm to the Pareto front.

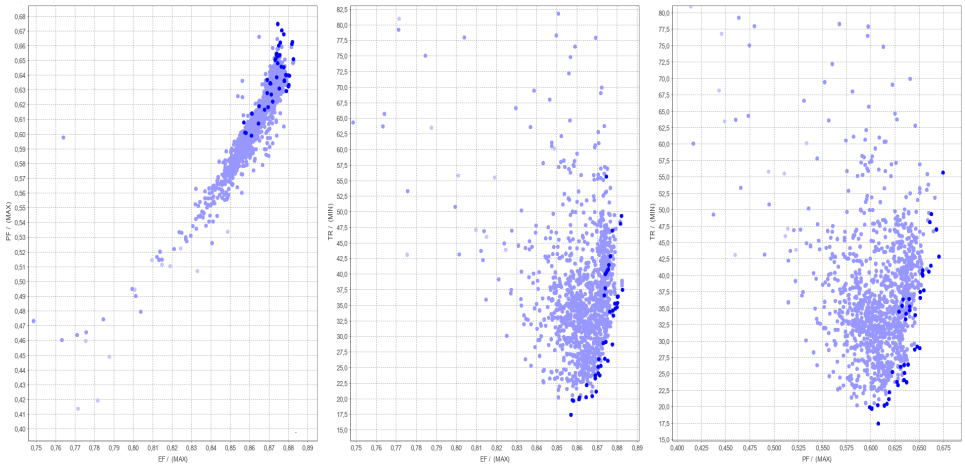

Figure 4.6: Memory archive in SyMSpace Optimizer.

The Pareto front with the best results is present in Fig. 4.7, Fig. 4.8 and Fig. 4.9. The objectives are efficiency, power factor and torque ripple. The torque ripple increases with

an increase in efficiency as it can be seen in Fig. 4.7. Also, the torque ripple increases with an increase in the power factor as it is shown in Fig. 4.8. The power factor vs efficiency is reported in Fig. 4.9. The power factor is quite unfortunate, but it is presumed about the LSSynRM with such a power. The machines with the bigger rated output power have a much better power factor, e.g. the LSSynRM with 30 kW can achieve power factor with value 0.838 [26]. The convergence to the best results can be seen in the first Fig. 4.7. There are the curves of individuals and their fitness increase with lower torque ripple and with an increase in efficiency. It is expected that with longer time of the optimization, it could be achieved better results. Two out of fourty four individuals suggested a possibility of better results. First is the individual with the lowest torque ripple and the second is individual with the higher efficiency. The possible curve, which could link up these two points, should bring even better solutions.

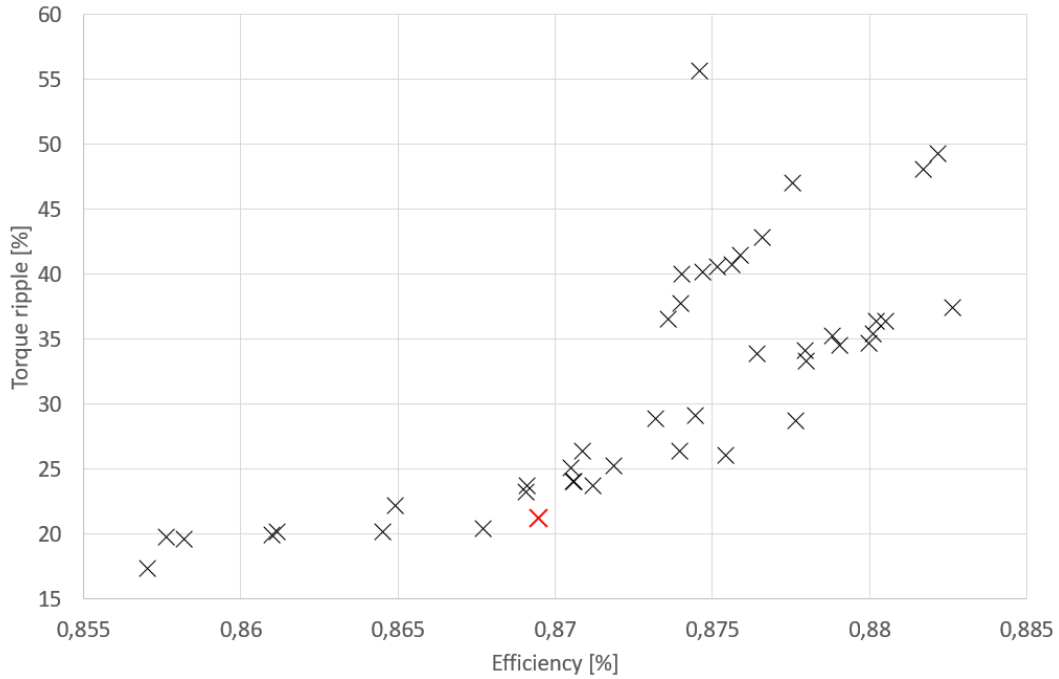

Figure 4.7: Torque ripple vs efficiency.

The one individual is selected for the detailed analysis. This individual is pointed up with red colour in Fig. 4.7, Fig. 4.8 and Fig. 4.9. The individual has acceptable torque ripple under 22 %. The estimated efficiency during optimization is electromagnetic, thus the mechanical losses are neglected. The electromagnetic efficiency of the chosen individual is 86.9 % and the power factor is 0.618. The IEC 60034-30 efficiency classification standard estimate IE3 efficiency for 4-pole 2.2 kW machine to 86.7 % and for IE4 the efficiency must be 89.5 %. It can be seen that the highest efficiency in optimization is 88,3 %, thus none of the individuals does reach so high efficiency to have IE4. The chosen individual, which can achieve IE3, is picked for detailed analysis.

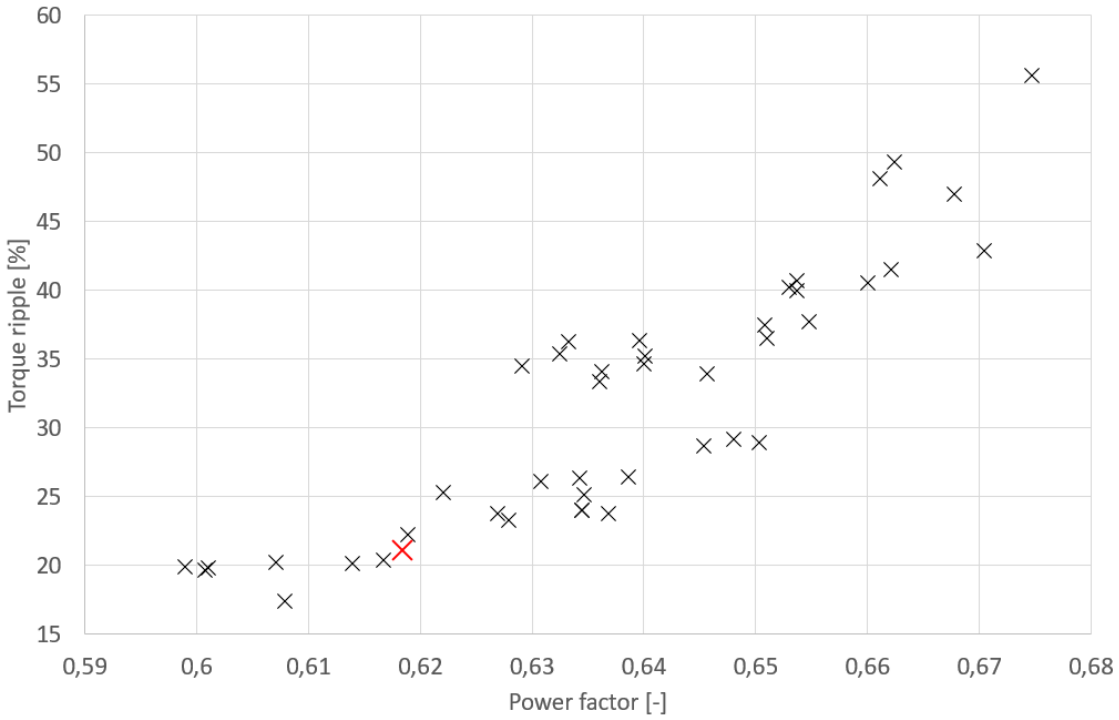

Figure 4.8: Torque ripple vs power factor.

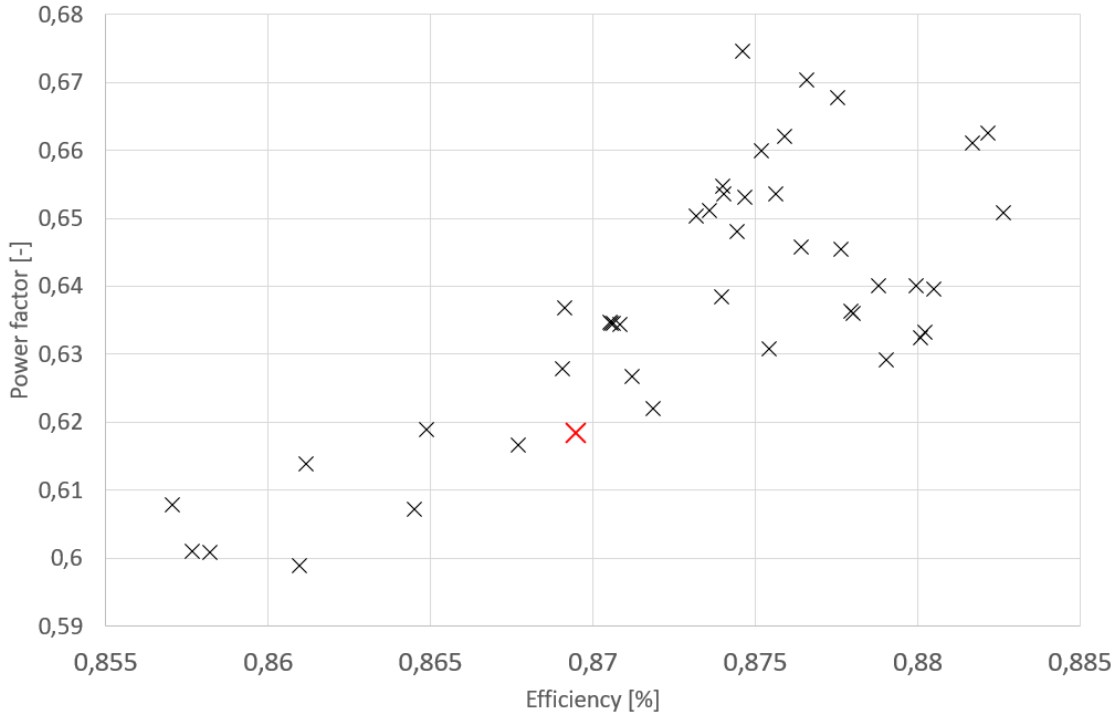

Figure 4.9: Power factor vs efficiency.

4.5 The optimized LSSynRM

The geometry of the chosen individual for comprehensive analysis is shown in Fig. 4.10. The yellow parts are aluminium and the bright blue part is iron sheet. It can be seen that the iron is united into one piece, which allows better mesh generation. The aluminium remains divided into the elements because there were obstacles to unite them too. The main problem is that the Ansys Maxwell demands more than one part for setting eddy currents. So the new algorithm for a searching number of singles surfaces of the aluminium. Normally the number would indicate the number of barriers, but as it can be seen in Fig. 4.10 there is one main barrier and then four smaller. The smaller barriers appear to be more like the bar of the squirrel cage.

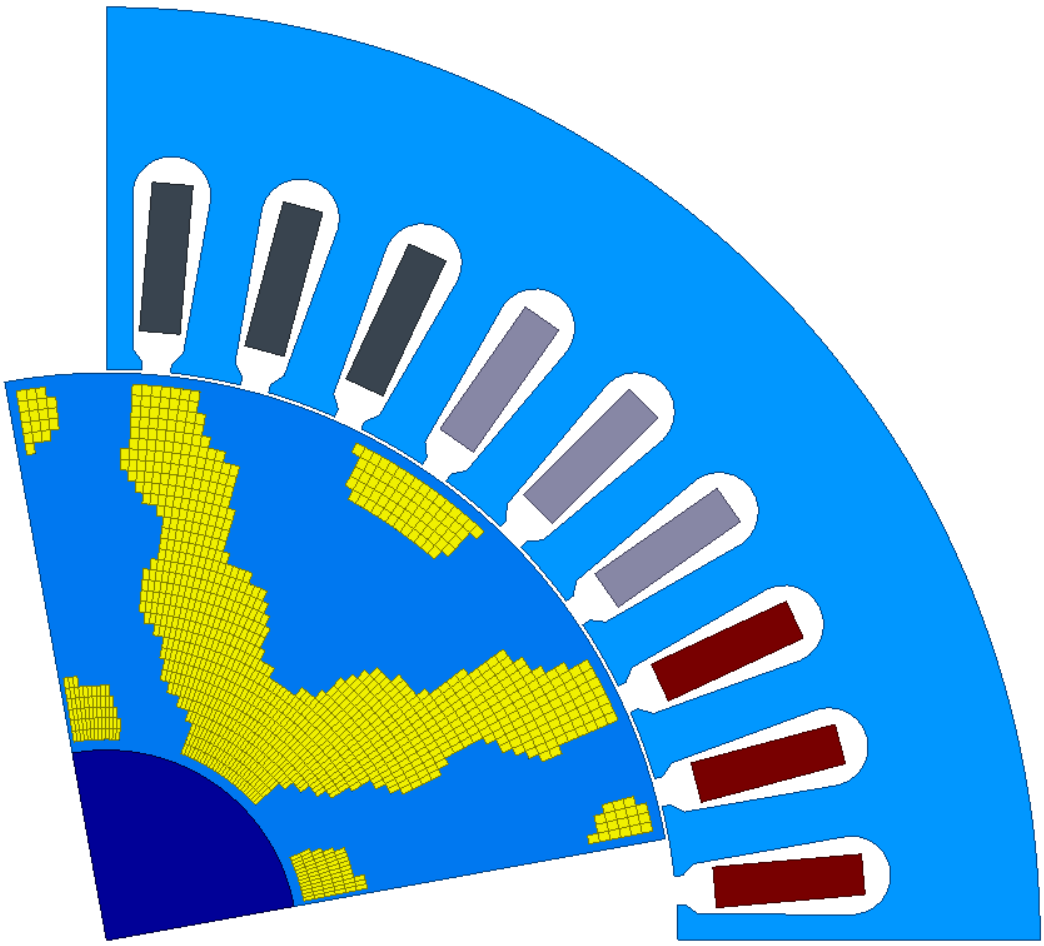

Figure 4.10: The geometry of the optimized LSSynRM for the detailed analysis.

The final mesh of the model in the Ansys Maxwell is shown in Fig. 4.11. The zoom to the inner area of rotor is shown in Fig. 4.11b. The mesh in the iron part has better distribution than in the aluminium parts. The mesh in the aluminium has not perfect distribution, because of the proportions of the elements. The generator of the mesh can not create a mesh with a larger distance between two nodes than the size of one element.

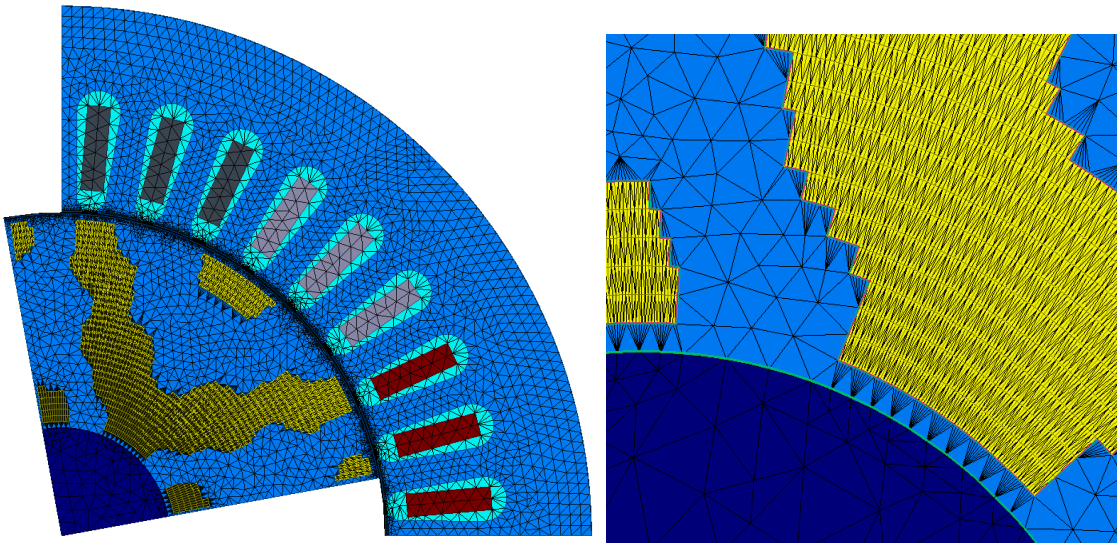

(a) The model of LSSynRM. **(b)** The zoom to the inner area of rotor.

Figure 4.11: Mesh grid of the model in Ansys Maxwell.

Thus, the mesh with an imperfect distribution is created. It was already mentioned that the unification of elements could bring better possibilities of mesh creation.

Table 4.3: Main parameters of LSSynRM in steady-state.

Parameter	Unit	Value
Apparent power, S	VA	3 903
Rated input power, P_1	W	2 411
Rated output power, P_2	W	2 214
Rated speed, n	rpm	1500
Line-to-line voltage, U_n	V	400
Rated phase current, $I_1 n$	A	5.627
Fundamental harmonic of flux density, B_{rad}	T	0.779
Power factor, $cos\varphi$	-	0.618
Estimated efficiency from losses, η	%	86.2
Estimated electromagnetic efficiency from losses, η_1	%	87.1
Efficiency from input/output ratio, η_2	%	91.8
Rated torque, T_n	Nm	14.099
Torque ripple peak to peak, T_{ripple}	Nm	5.945
Torque ripple, T_{ripple}	%	21.084
Synchronous inductance in d-axis, L_d	mH	0.220
Synchronous inductance in q-axis, L_q	mH	0.052
Saliency ratio, L_d/L_q	-	4.230

The main parameters of line-start synchronous reluctance motor are shown in Ta-

ble 4.3. The rated output power of the motor is 2.2 kW and the rated speed is 1500 rpm. The low power factor 0.618 results in a higher rated phase current of the value 5.6 A. The estimated efficiency from losses is 86.2 % and the estimated electromagnetic efficiency also estimated from losses is 87.1 %. The difference between the initially estimated electromagnetic efficiency of 86.9 % and the estimated electromagnetic efficiency 87.1 % is affected by the time step in the analysis. The time step 0.1 ms is used in the detailed analysis against 0.2 ms in transient analysis during optimization. The efficiency estimated from input and output power ratio is 91.8 %.

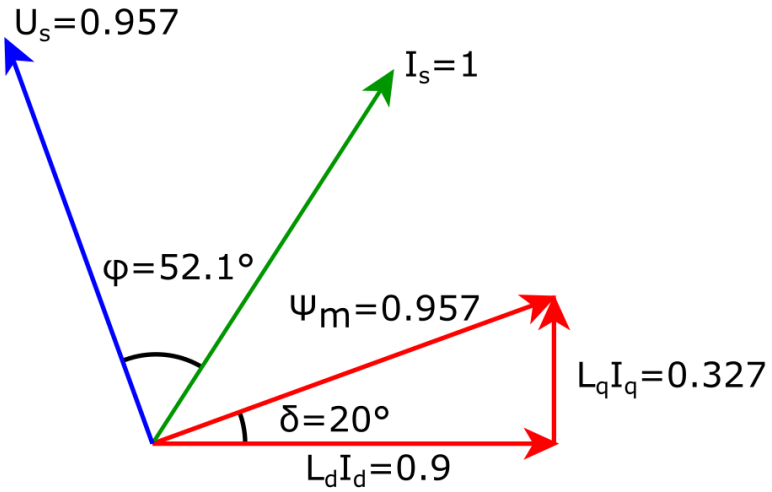

Figure 4.12: Phasor diagram at steady-state.

Rated torque is 14.1 Nm and torque ripple is 21.1 %. The saliency ratio is 4.23, which is quite poor value. The saliency ratio normally reaches about 10.00 in TLA [3]. The saliency ratio with a value almost 12.00 is achieved in [26]. In Fig. 4.12 the phasor diagram of the LSSynRM at steady-state can be seen.

Table 4.4: The distribution of losses in steady-state.

Parameter	Unit	Value
Iron losses, P_{Fe}	W	95.359
Solid losses, P_{Solid}	W	16.808
Stator resistive losses, P_{CuS}	W	221.415
Mechanical losses, P_{Mech}	W	22.000
Extra losses, P_{Extra}	W	0.221
Sum of losses, P_{Sum}	W	355.802

The distribution of losses in steady-state is shown in Table 4.4. Fig. 4.13 illustrates the distribution of losses in percentages. The biggest portion of losses 62.2 % is created by stator resistive losses. It is caused by high stator currents due to low power factor.

Core losses present 26.8 % and the solid losses are 4.7 %. Mechanical losses are set to 22 W and it is 6.2 %.

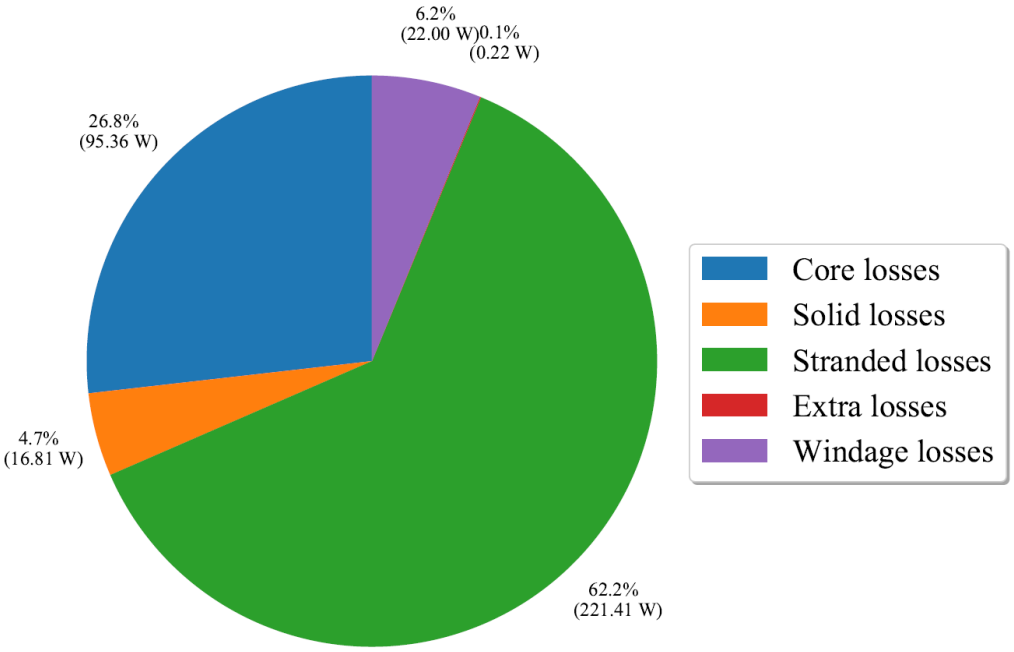

Figure 4.13: Distribution of losses.

The losses behaviour at the steady-state can be seen in Fig. 4.14. The stator resistive losses grow bigger against the stator resistive losses in initial induction motor with the same stator due to increase of the stator current.

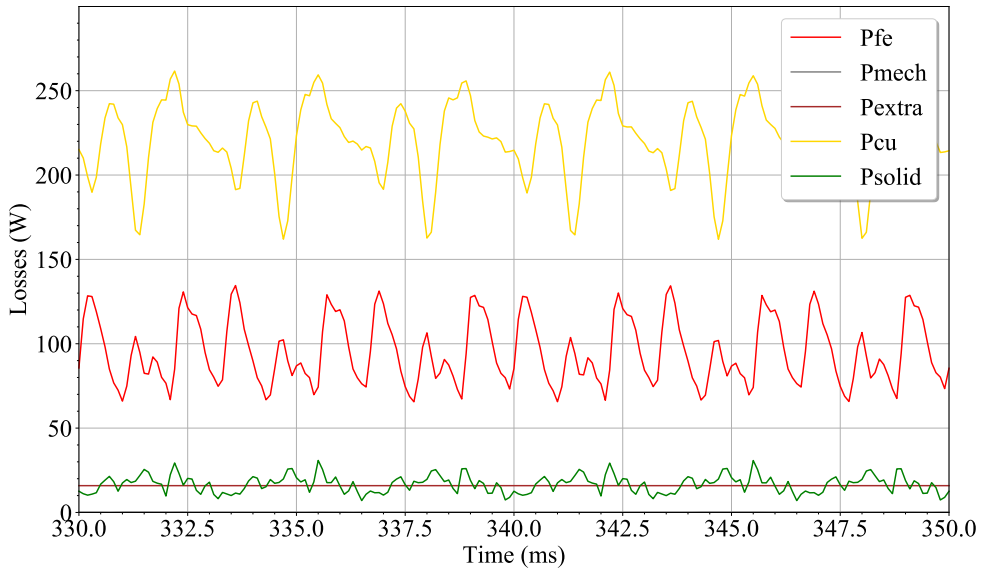

Figure 4.14: Losses behavior at steady-state.

4.5.1 Starting process

The synchronization capability is the main reason, why the transient analysis is required. The transient analysis is performed for obtaining transients line of speed, torque, currents etc. The load mass of inertia is equal to the rotor mass of inertia. The speed waveform is shown in Fig. 4.15. The speed of 1 500 rpm is reached in 145 ms. The synchronization is in 200 ms after slight overshoot. The LSSynRM reaches synchronous speed, so the synchronization is successful.

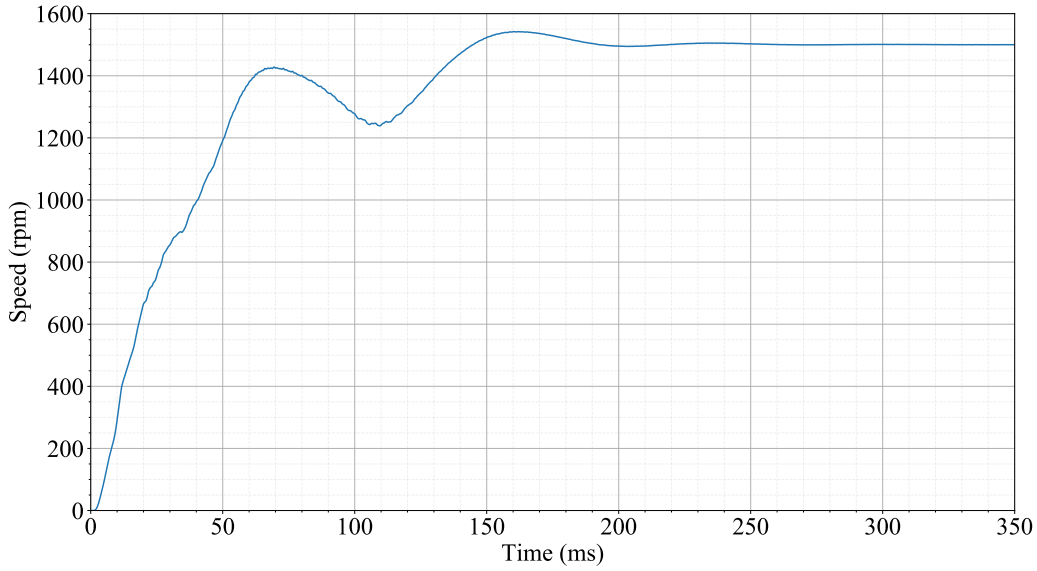

Figure 4.15: Speed dependency on time during the starting process.

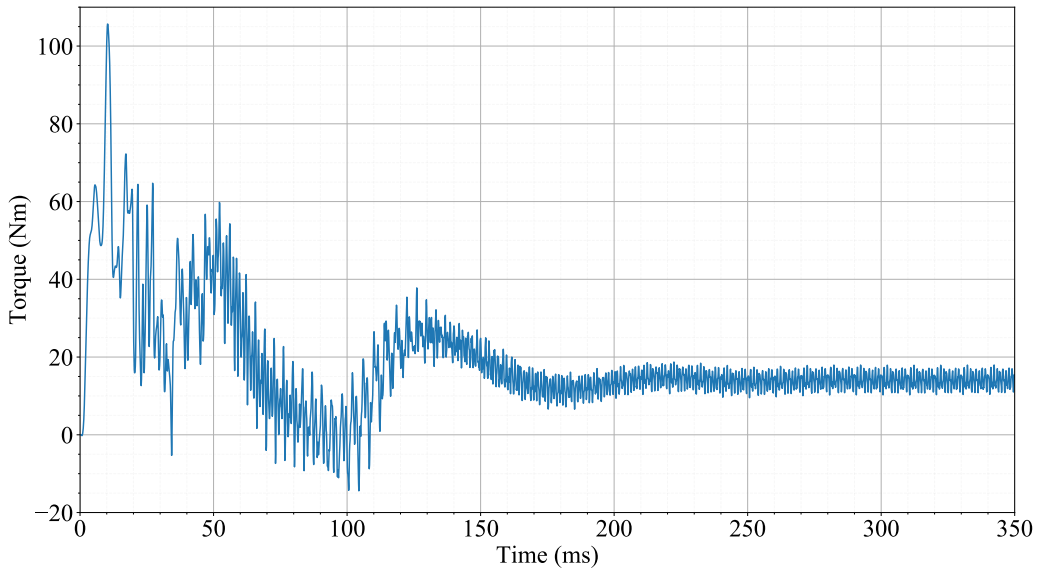

Figure 4.16: Torque dependency on time during the starting process.

Fig. 4.16 shows the torque during the starting process. Torque stabilizes at the value of 14.1 Nm in 200 ms. Fig. 4.17 shows torque vs speed. It can be seen that the motor successfully reach synchronization at rated torque.

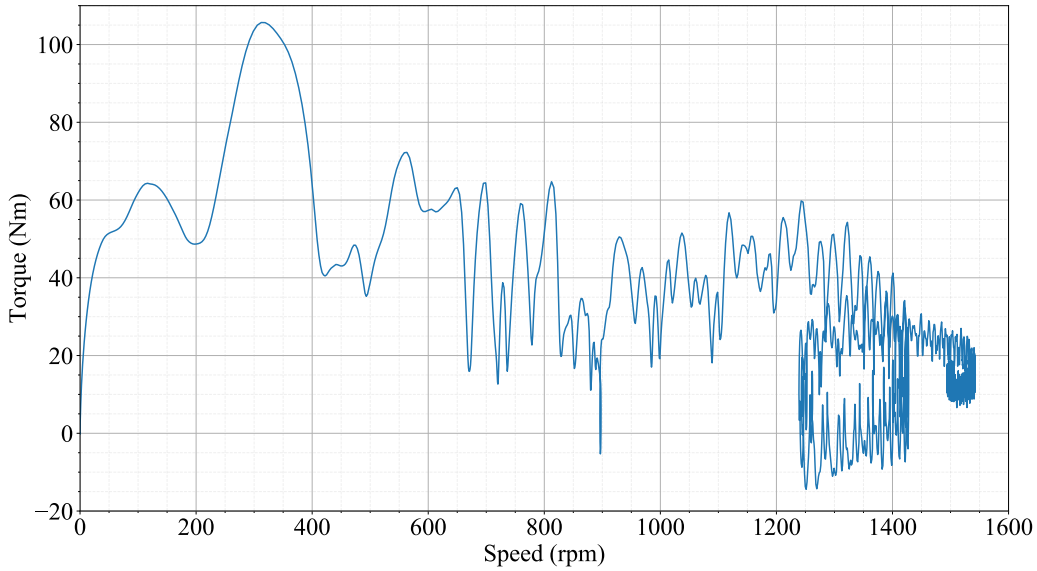

Figure 4.17: Torque dependency on speed.

The waveforms of phase currents during the starting process are shown in Fig. 4.18. The maximal current is 58.6 A, which is approximately ten times higher compared to the rated current.

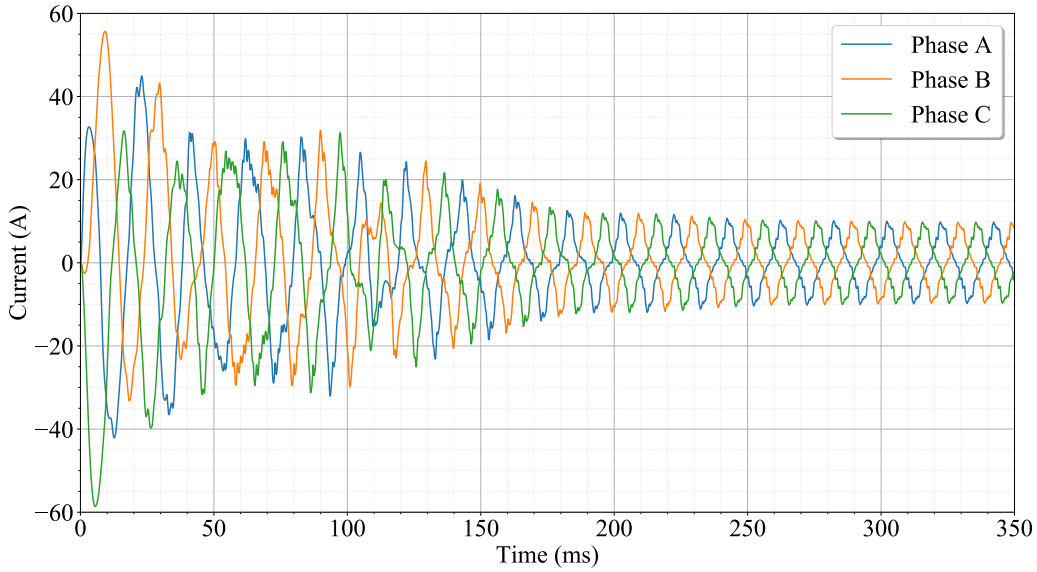

Figure 4.18: Phase currents dependency on time during the starting process.

4.5.2 Behavior at steady-state

The flux density distribution is shown in Fig. 4.19. The ribs on the surface of the rotor are the most saturated parts. The calculated flux density in this area reaches almost 2.3 T. Also, the area between the main barrier and the not-central bar is saturated. The flux density in this area is about 1.9 T. The saturation of these parts leads to lower flux density in the air gap and thus to the lower electromagnetic torque. The flux density in the yoke of the stator is 1.5 T and in the stator teeth is 1.8 T. The calculated flux density in the inner area of the rotor between the main barrier and the ”bars” is 1.8 T. The removal of the inner ”bars” would lead to lower flux density in this area. On the other hand, it could change the saliency ratio of the rotor and it could lead to lower torque.

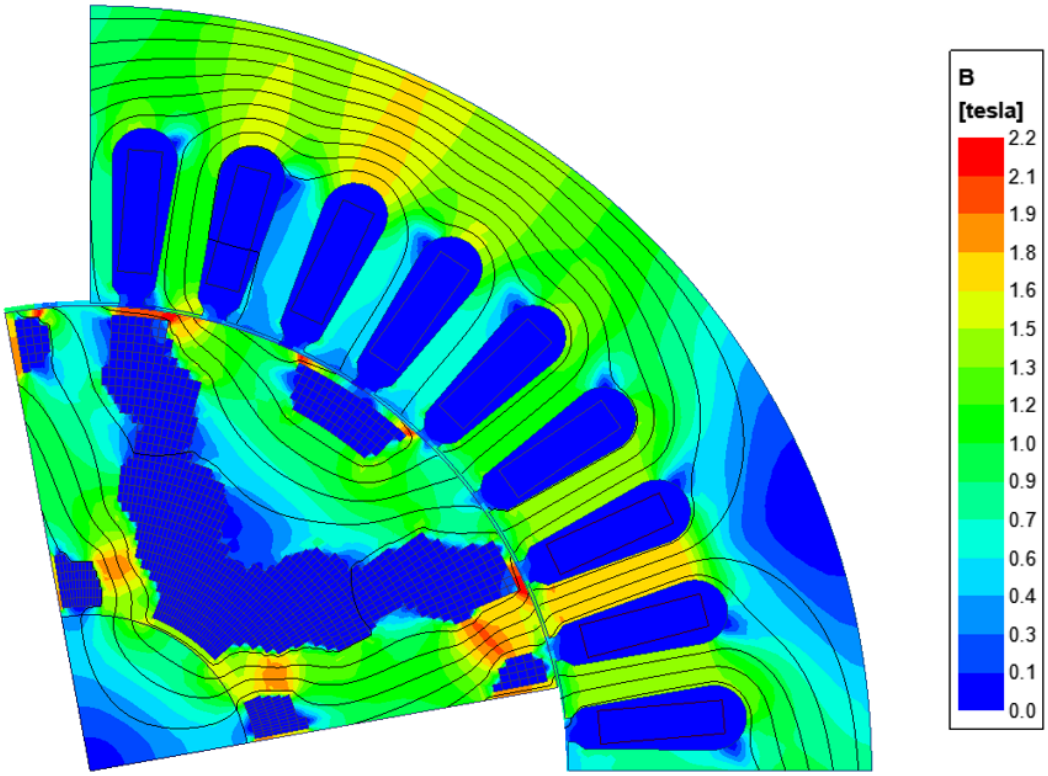

Figure 4.19: Flux density distribution in the LSSynRM.

The magnetic flux density in the middle of the air gap vs periphery length is shown in Fig. 4.20. The length of the air gap in one-quarter of the rotor is 70.7 mm, thus Fig. 4.20 shows the magnetic flux in the middle of the air gap in one-quarter of the rotor. It can be seen that the flux ripple is significant due to the higher harmonics presence. The harmonics are expected with a low number of slotting in the rotor. Moreover, the distance between barrier and the bars is quite large which also leads to a ripple of flux density.

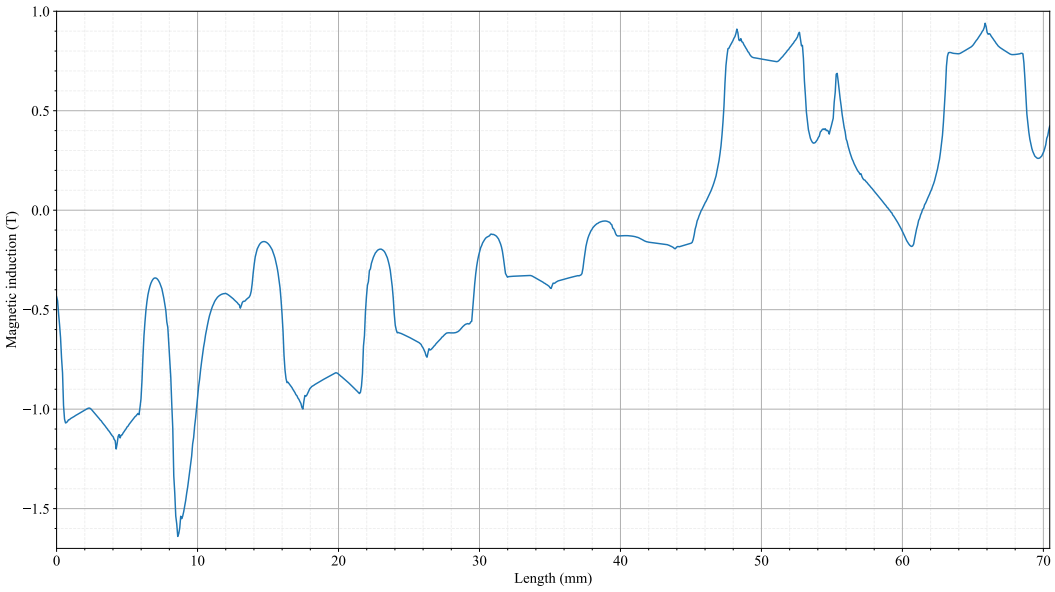

Figure 4.20: Magnetic flux density in the middle of the air gap.

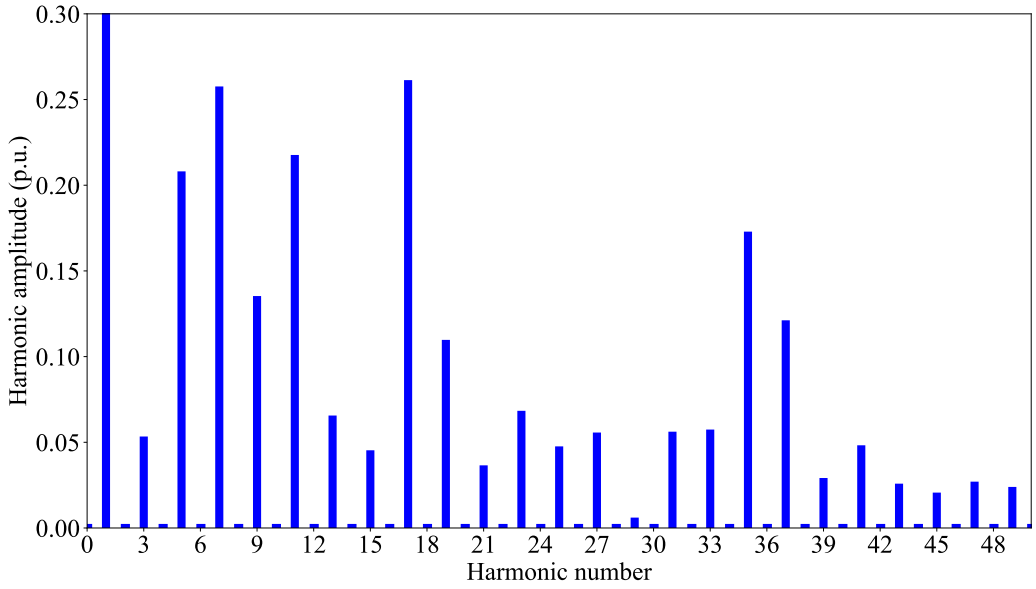

Figure 4.21: Normalized harmonic content of flux density normal component.

The FFT analysis is performed to obtain harmonic content of flux density in the middle of the air gap. Fig. 4.21 displays the results of the FFT analysis and the harmonic amplitudes are in p.u. Mainly the harmonic content depends on the geometry and the number of stator and rotor slots. In the FFT the harmonics around 36, 18 and 9 are present because the number of stator slots is 36. The number of rotors ”bars” is 20. The number of rotors ”bars” could be also proclaimed as 16 if the ”bars” on the edges of the poles are joint due to thin bridge between them. The harmonics numbers depending on

a number of the rotors ”bars” are also noticeable. The first harmonic of flux density in air gap is 0.78 T. Total harmonic distortion THD of the magnetic flux density in the middle of air gap is 52.4 % and it indicates that the rotor geometry is not very good. Of course, the current harmonic content affects the flux distribution in the middle of the air gap too.

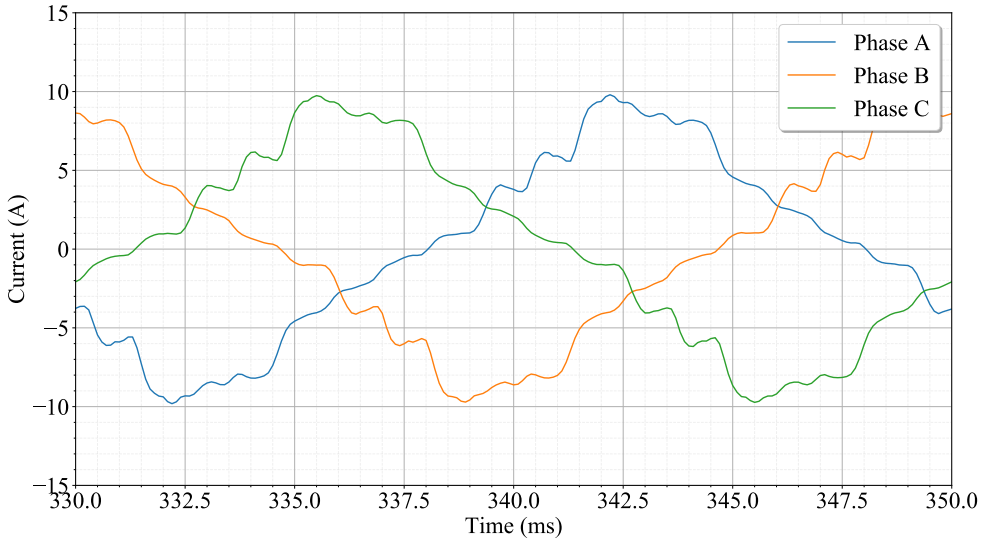

Figure 4.22: Currents behavior at steady-state.

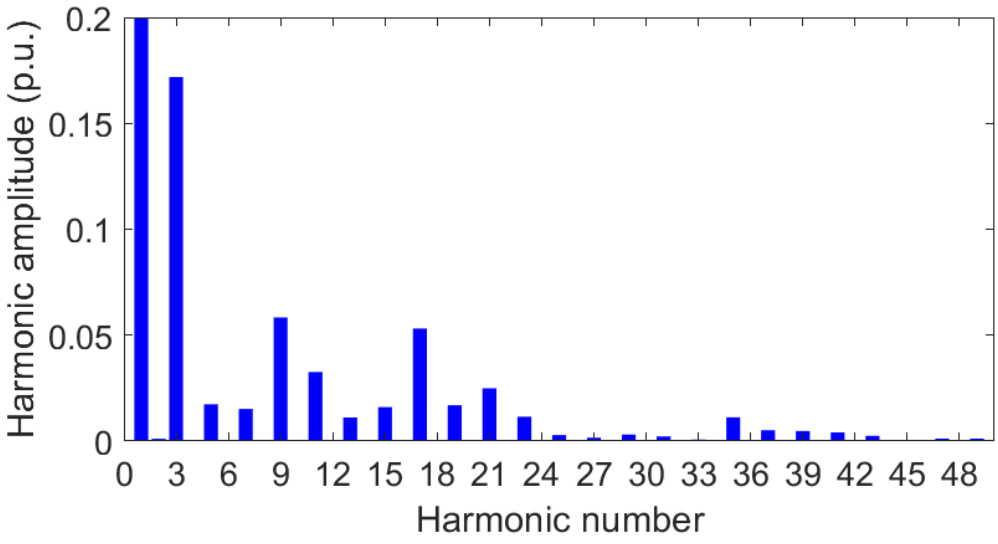

Figure 4.23: Normalized harmonic content of the phase current.

The waveform of phase currents at steady-state is shown in Fig. 4.22. The FFT analysis of phase currents at steady-state is shown in Fig. 4.23. The harmonic content of the currents has always same content in three-phase winding: 5, 7, 11, 13, 17, 19, 23, 25, 29,

31, 35, 37, 41, 43 and higher harmonics [33]. The third harmonic has the most significant harmonic amplitude and it is 17 % of the first harmonic number. Such high value of the third harmonic is present due to the saturation of the motor. THD of the current is 19.6 %. In Fig. 4.23 it can be seen that these harmonics are presented. Once again, the harmonics around 18 and 36 are affected by the number of stator slots. The [33] recommends safe choices of the combination of the number of rotor slots depending on the number of stator slot. As it was already mentioned the number of rotors "bars" is 16 or 20. Both of these numbers of rotors "bars" creates harmful torques. The lowest number of rotor bars should be 24 according to 36 stator slots.

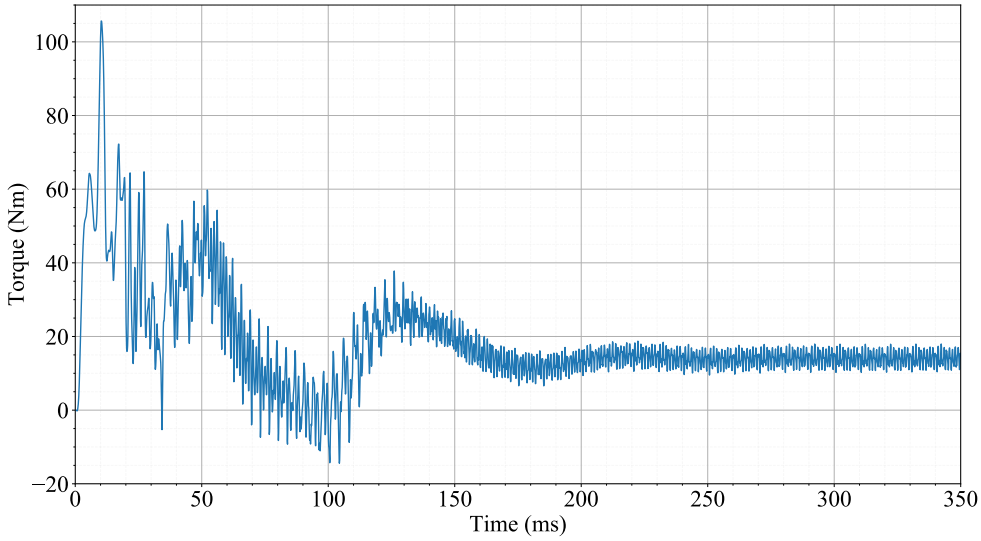

Figure 4.24: Torque behavior at steady-state.

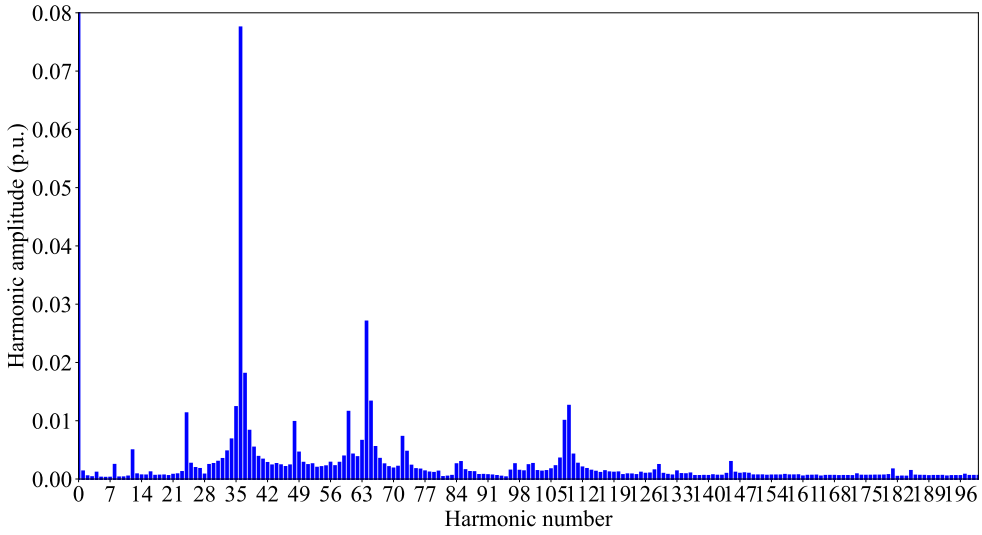

Figure 4.25: Normalized harmonic content of torque.

The torque behaviour at steady-state is shown in Fig. 4.24 and its FFT analysis in Fig. 4.25. The normalized harmonic of the torque is in p.u. to the average value of 14.1 Nm. The higher harmonics almost reach 10 % in p.u. The torque ripple is 21.1 %.

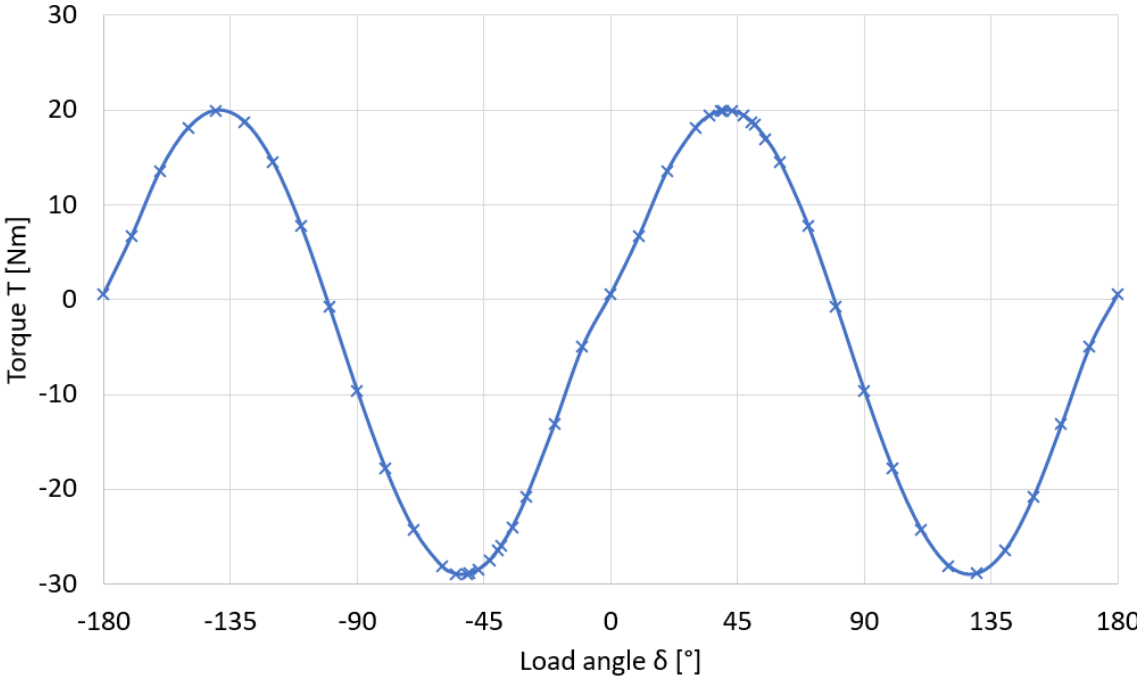

Figure 4.26: Load angle vs torque.

The analysis of dependency of torque on the load angle is performed and the results are shown in Fig. 4.26. The results show the reluctance moment according to the load angle. The maximum torque is 20 Nm and it is near to 45° of load angle. The load angle in steady-state is 20° which leads to torque with a value of 14 Nm.

4.5.3 Comparison of optimized LSSynRM with prototypes showed in [4]

Table 4.5 shows a comparison of optimized LSSynRM in this master thesis, IM with the same stator and LSSynRMs presented in [4]. The comparison with prototypes showed in [4] is chosen because the presented prototypes have equal rated output power. On first sight, the LSSynRM has better efficiency than any of the proposed prototyped in LSSynRM. On the other hand, it has the worst power factor. The prototypes are based on IM with efficiency 79.0 % and power factor 0.794. It can be seen that the prototypes LS2 and LS3 achieved better performance than their initial IM and LS1 got worst performance, especially due to increasing of stator current.

The comparison of these motors is shown mainly because of the geometries, which can be seen in Fig. 4.27. The optimized LSSynRM in this thesis is mostly alike the prototype LS1. It is clear from the comparison that the LS1 with two flux barriers has the

worst performance against the LS2 and LS3. The same phenomenon is also presented in [26]. The [26] analyse how the number of flux barriers affects the final performance of the motor. The motors with rated output power 30 kW, shows the same tendency of increase of efficiency with the increasing number of flux barriers up to five.

Table 4.5: Comparison of optimized LSSynRM, initial IM and LSSynRMs [4].

		LSSynRM	IM	LS1	LS2	LS3
P_2	W	2 214	2 217	2 231	2 231	2 231
n	rpm	1 500	1 464	1 500	1 500	1 500
T_n	Nm	14.1	14.5	14.2	14.2	14.2
U_n	V	400	400	400	400	400
$I_1 n$	A	5.627	4.31	5.80	4.79	4.95
$cos\varphi$	-	0.618	0.808	0.718	0.763	0.745
η	%	86.2	86.6	77.3	84.5	83.4

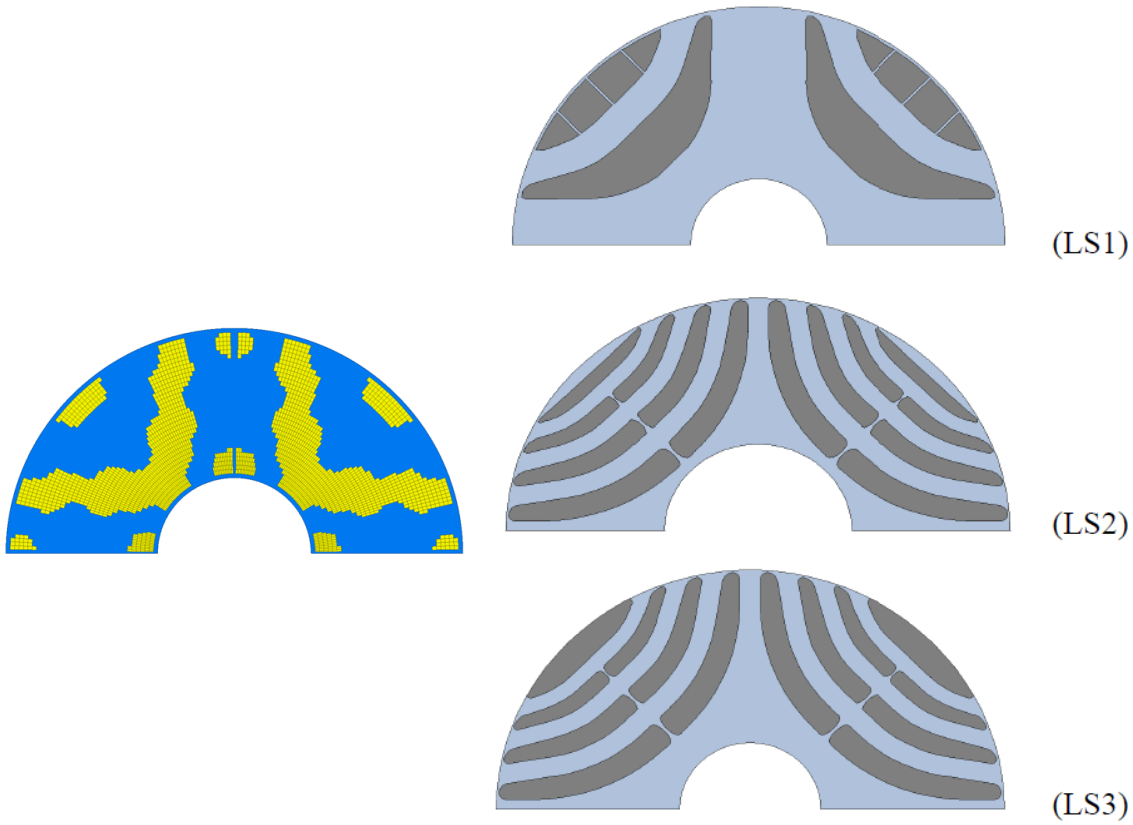

(a) The final LSSynRM of the optimization. **(b)** Design choices presented in [4].

Figure 4.27: The geometries selected for comparison.

It is expected that it could be achieved much better results with the distribution of Gaussian functions in NGnet that could allow geometries with more than two barriers.

The most obvious idea to reach that objective is the increase in the number of Gaussians in the designed space.

The other plan is the relocation of the inner boundaries of Gaussians. As it can be seen in the final geometry (see Fig. 4.27a) the flux barriers fully touch the shaft if we dismiss the thin bridge. It is clear that the barrier should be moved in the direction to the outer area of the rotor to allows more beneficial magnetic flux distribution in this area. The possible movement of the inner barrier of Gaussians should prevent flux barrier position exactly next to the shaft.

Also, one of the ideas is gradually growing of Gaussians variance σ. The Gaussian functions in the inner area of the rotor can have a wider variance σ than the Gaussians in the outer area of the rotor. The gradually growing smaller in direction to the outer area of the rotor would be ideal. This approach could bring better representation ability in the outer area of the rotor with a potential reasonable number of Gaussian functions.

Conclusion

This master thesis deals with topology optimization of the line-start synchronous machines. The topology optimization offers a new way to the machines performance improvement. The comparison between direct topology optimization and shape optimization also called as the parametric optimization, is presented in the first chapter. The main benefit of topology optimization is the final optimized geometry free of almost any constraints. The geometry created by topology optimization can suggest a more desirable solution then parametric optimization for a specific task such as minimizing of torque ripple or maximizing of output power. The parametric optimization of shape suggested by DTO can be performed to achieve the best possible performance of the motor. On the other hand, further parametric optimization is not essential, because in [15] the optimized final wavy shape was directly simplified for productions without further parametric optimization and the simplification gives no significant effects on the performance.

The line-start synchronous reluctance machine is chosen as the possible replacement of induction motors with reducing electricity consumption goal in this master thesis. The second chapter describes the construction and operation principle of such a motor. The LSSynRM is a hybrid of induction motor and synchronous reluctance motor and it joints the positive feature from both of them. It can start directly on the line as the induction motor and it shows better performance in synchronous steady-state after synchronization than the induction motor, especially in the efficiency.

The third chapter presents the analysis of possible concepts for characterizing the investigated and optimized design space. Firstly the created model in Ansys Maxwell is described and the theory of the normalized Gaussian network is explained. This chapter mainly focuses on the deployment of Gaussian functions in the normalized Gaussian network. It shows the different version of Gaussians distributions in designed space and in NGnet. After achieving the equal Gaussians distribution in the entire rotor, the dependency of Gaussians variance σ and overleap Ω on the final NGnet is studied. The final distribution of Gaussian functions in NGnet used during optimization is presented at the end of this chapter.

Topology optimization of line-start synchronous reluctance motor based on the normalized Gaussian network is described in the last chapter. This chapter includes a description of SyMSpace project for topology optimization of LSSynRM and also a description of SyMSpace Optimizer setting which is used during optimization in this master thesis. The main part of this chapter deals with the created evaluation algorithm of a single individual. It was discovered during work on the master thesis that the creation of this evaluation algorithm is necessary, because the transient analysis, which is required for analysis LSSynRM, demands an enormous amount of time. This is presumably the rea-

son why the papers about topology optimization deal exclusively with synchronous machines, where the steady-state analysis is sufficient. Thus, this master thesis deals with the unexplored field of topology optimization of the line-start machines. The transient analysis takes approximately 2-3 hours for each individual and the main purpose of the evaluation algorithm is to prevent performing of the time consuming transient analysis with the unfeasible or unsatisfying geometries. If the geometry is restricted in the first step due to unfeasible geometry the evaluation algorithm needs approximately 5 minutes. If the geometry is sorted out due to unsatisfying torque the evaluation algorithm takes around 30 minutes. Thus, the evaluating of unfeasible geometries is reduced from 2-3 hours to 5-30 minutes. Thus, thanks to the evolved algorithm the exceptional reduction of optimization time is reached.

Further, the last chapter presents Pareto front obtained by the topology optimization, which ran for one and half month. It is expected that with longer time of the optimization, that better results could be achieved. Two out of fourty four individuals in Pareto front suggested a possibility of better results. The one individual with potential to accomplish IE3 is picked for the detailed analysis. Unfortunately, the comprehensive analysis of the individual shows that the optimized LSSynRM has efficiency only 86.2 % and thus it would be recognized as the IE2. Also, the performance got worst against the initial induction motor with the same stator. On the other hand, it achieved better efficiency than the LSSynRMs (LS1, LS2 and LS3) with equal rated output power presented in [4]. The [4] and [26] shows that satisfactory efficiency can be obtained only with an increase in the number of flux barriers. Therefore, the solver in the SyMSpace Optimizer needs NGnet with higher variability resulting in more complicated and dissected shapes of the rotor.

The topic of topology optimization is very progressive and in combination with line-start motors, it becomes very challenging. The created evaluating algorithm can be used for future work. The further improvements of the Gaussians distribution in NGnet following the suggestions of this master thesis should be done in the future doctoral thesis. The doctoral thesis could also obtain topology optimization considering localized material degradation caused by manufacturing [34], [35] and [36]. Moreover, the topology optimization of the single-phase line-start synchronous machine could be performed.

Referencess

[1] A. T. de Almeida, F. J. T. E. Ferreira, and G. Baoming. "*Beyond Induction Motors—Technology Trends to Move Up Efficiency*". In: *IEEE Transactions on Industry Applications*. Vol. 50. (3). IEEE, 2014, pp. 2103–2114. DOI: https://doi.org/10.1109/TIA.2013.22884257.

[2] I. Lolová. "Design of super premium efficiency line-start permanent magnet synchronous machine". In: *Proceedings of the 25th Conference STUDENT EEICT 2019*. Brno University of Technology, Faculty of Electrical Engineering and Communication: IEEE, 2019, pp. 228–231. ISBN: 978-80-214-5735-5.

[3] Valerii Abramenko. *Synchronous reluctance motor in direct online applications*. Lappeenranta, 2016.

[4] M. GAMBA et al. "Design of a line-start synchronous reluctance motor". In: *2013 International Electric Machines & Drives Conference*. IEEE, 2013, pp. 648–6557. ISBN: 978-1-4673-4974-1. DOI: 10.1109/IEMDC.2013.6556163.

[5] A.-C.ZĂVOIANU et al. "*Multi-objective topology optimization of electrical machine designs using evolutionary algorithms with discrete and real encodings*". In: *Computer Aided Systems Theory – EUROCAST 2017*. Cham: Springer, 2018, pp. 331–338. ISBN: 978-3-319-74718-7. DOI: https://doi.org/10.1007/978-3-319-74718-7_40.

[6] I. ZELINKA. *Umělá inteligence v problémech globální optimalizace*. 1st ed. Prague: BEN, 2002, p. 189. ISBN: 80-7300-069-5.

[7] E. VOLNÁ. *Evoluční algoritmy a neuronové sítě*. 1st ed. Ostrava: Ostravská univerzita, 2012, p. 152. URL: http://www1.osu.cz/~volna/Evolucni_algoritmy_a_neuronove_site.pdf.

[8] L. DE GIOVANNI. *Methods and Models for Combinatorial Optimization: Heuristis for Combinatorial Optimization[online]*. Padova: Italy: The University of Padova, 2016, p. 15. URL: http://www.math.unipd.it/~luigi/courses/metmodoc1617/m02.meta.en.partial01.pdf.

[9] E. ELBELTAGI, T. HEGAZY, and D. GRIERSON. "Comparison among five evolutionary-based optimization algorithms". In: *Advanced Engineering Informatics [online]*. Vol. 19(1). Elsevier, 2005. DOI: 10.1016/j.aei.2005.01.004.

[10] D. DAVENDRA and I. ZELINKA. *Self-Organizing Migrating Algorithm Methodology and Implementation, Studies in Computational Intelligence Volume 626*. Springer, 2016, p. 289. ISBN: 978-3-31-928161-2. DOI: 10.1007/978-3-319-28161-2.

[11] T. BÄCK, D. B. FOGEL, and Z. MICHALEWICZ. *Handbook of Evolutionary Computation*. United Kingdom: Ltd.Techno House Redcliffe Way Bristol, 1997, p. 988. ISBN: 978-0-7503-0392-7.

[12] T. BÄCK. *Evolutionary Algorithms in Theory and Practice*. New York: Oxford University Press, 1996. ISBN: 978-0-19-509971-3.

[13] M. TULEJA. *GENETIC ALGORITHMS - IMPLEMENTATION OF MULTIPROCESSING*. MASTER'S THESIS, Supervisor: V. OUJEZSKÝ. Brno: BUT: Brno University of Technology, 2018, p. 77. URL: https://www.vutbr.cz/www_base/zav_prace_soubor_verejne.php?file_id=172844.

[14] J. KENNEDY and R. EBERHART. "Particle Swarm Optimization". In: *Proceedings of the IEEE international conference on neural networks*. Washington: IEEE Service Center, 1995, pp. 1942–1948. ISBN: 0-7803-2768-3.

[15] Shunpei SATO, Takahiro SATO, and Hajime IGARASHI. "Topology Optimization of Synchronous Reluctance Motor Using Normalized Gaussian Network". In: *IEEE Transactions on Magnetics*. Vol. 51(3). IEEE, 2015. DOI: 10.1109/TMAG.2014.2359679.

[16] Takahiro SATO, Kota WATANABE, and Hajime IGARASHI. "Multimaterial topology Optimization of Electric Machines Based on Normalized Gaussian Network". In: *IEEE Transactions on Magnetics*. Vol. 51(3). IEEE, 2015. DOI: 10.1109/TMAG.2014.2359972.

[17] Ondřej VÍTEK. "Synchronní reluktanční motory: přednášky Elektrické pohony MEMI, VUT FEKT [online]".

[18] M. GAMBA et al. "Line-start synchronous reluctance motors: Design Guidelines and Testing via Active Inertia Emulation". In: *2015 IEEE Energy Conversion Congress and Exposition (ECCE)*. IEEE, 2015, pp. 4820–4827. ISBN: 978-1-467-37150-6. DOI: https://doi.org/10.1109/ECCE.2015.7310340.

[19] V. ABRAMENKO, I. PETROV, and J. PYRHÖNEN. "Analysis of damper winding designs for direct-on-line synchronous reluctance motor". In: *IECON 2017 - 43rd Annual Conference of the IEEE Industrial Electronics Society*. Vol. 1. Lappeenranta, Finland: IEEE, 2017, pp. 320–326. ISBN: 978-1-5386-1127-2. DOI: 10.1109/IECON.2017.8216305.

[20] K. TANG et al. “Rotor Design and Optimization of the Single-phase Line-start Synchronous Reluctance Motor”. In: *2017 20th International Conference on Electrical Machines and Systems (ICEMS)*. China: IEEE, 2017. ISBN: 978-1-5386-3246-8. DOI: 10.1109/ICEMS.2017.8056082.

[21] T. JUNG et al. “The Rotor Conductor Design for Starting Stability of Line-Start Synchronous Reluctance Motor”. In: *IECON 2006 - 32nd Annual Conference on IEEE Industrial Electronics*. China: IEEE, 2006. ISBN: 978-1-5090-9155-3. DOI: 10.1109/IECON.2006.347605.

[22] TAE-UK JUNG and HYUK NAM. “The Rotor Conductor Design for Starting Stability of Line-Start Synchronous Reluctance Motor”. In: *Journal of Electrical Engineering & Technology*. Vol. 1. Paris, France, 2006, pp. 320–326. DOI: 10.5370/JEET.2006.1.3.320.

[23] V. Hrabovcová and M. Ličko. *Reluktančný synchrónny motor*. Žilina: Žilinská univerzita, 2001, p. 229. ISBN: 80-7100-891-5.

[24] J.R. HENDERSHOT and T.J.E. MILLER. *Design of brushless permanent - magnet machines*. 2nd ed. Florida: Motor Design Books LLC : Venice, 2010, p. 798. ISBN: 978-0-9840687-0-8.

[25] Valerii Abramenko, Ilya Petrov, and Juha Pyrhonen. “Analysis of damper winding designs for direct-on-line synchronous reluctance motor”. In: *IECON 2017 - 43rd Annual Conference of the IEEE Industrial Electronics Society [online]*. IEE, 2017, pp. 1802–1809. DOI: https://doi.org/10.1109/IECON.2017.8216305.

[26] Valerii Abramenko et al. “Design Aspects of Direct-on-Line Synchronous Reluctance Motors”. In: *2018 XIII International Conference on Electrical Machines (ICEM)*. ICEM, 2018, pp. 138–145. ISBN: 978-1-538-62477-7. DOI: https://doi.org/10.1109/ICELMACH.2018.8506710.

[27] Seung-Do Han, Hyoun-Jeong Shin, and Jun-Ho Ahn. *Line start reluctance synchronous motor*. Patent US 7,161,270 B2. Jan. 2007. URL: https://patents.google.com/patent/US7161270B2/en?oq=EP+1524755+A1.

[28] S. SILBER et al. “*Reducing Development Time of Electric Machines with SyMSpace*”. In: *2018 8th International Electric Drives Production Conference (EDPC) [online]*. IEEE, 2018, pp. 1–5. ISBN: 978-1-728-10147-7. DOI: https://doi.org/10.1109/EDPC.2018.8658312.

[29] S. SILBER et al. “*A fast and elitist multiobjective genetic algorithm: NSGA-II*”. In: *IEEE Transactions on Evolutionary Computation*. Vol. 6. IEEE, 2002, pp. 182–197. DOI: https://doi.org/10.1109/4235.996017.

[30] A.-C.ZĂVOIANU et al. "*Hybridization of multi-objective evolutionary algorithms and artificial neural networks for optimizing the performance of electrical drives*". In: *Engineering Applications of Artificial Intelligence [online]*. Vol. 26(8). Elsevier, 2013, pp. 1781–1794. DOI: https://doi.org/10.1016/j.engappai.2013.06.002.

[31] E. ZITZLER and M. LAUMANNS. "*SPEA2: Improving the strength pareto evolutionary algorithm*". In: TIK-report (103), 2001. DOI: https://doi.org/10.3929/ethz-a-004284029.

[32] A.-C.ZĂVOIANU et al. "DECMO2: A robust hybrid and adaptive multi-objective evolutionary algorithm". In: *Soft Comput.* Vol. 19. Springer, 2015, pp. 3551–3569. DOI: 10.1007/s00500-014-1308-7.

[33] J. PYRHÖNEN, T. JOKINEN, and V. HRABOVCOVÁ. *Design of rotating electrical machines. Second edition.* 2nd ed. Chichester, West Sussex: WIley, 2014. ISBN: 978-1-118-70162-1.

[34] Y. Hidaka and H. Igarashi. "*Topology Optimization of Synchronous Reluctance Motors Considering Localized Magnetic Degradation Caused by Punching*". In: *IEEE Transactions on Magnetics*. Vol. 51. (6). IEEE, 2017, pp. 1–4. DOI: https://doi.org/10.1109/TMAG.2017.2659721.

[35] Y. Hidaka, S. Furui, and H. Igarashi. "*Robust Optimization Considering Probabilistic Magnetic Degradation*". In: *IEEE Transactions on Magnetics*. Vol. 51. (3). IEEE, 2015, pp. 1–4. DOI: https://doi.org/10.1109/TMAG.2014.2353653.

[36] Y. Hidaka and H. Igarashi. "*Topology optimization of rotating machine rotors considering localized magnetic degradation caused in manufacturing process*". In: *2016 IEEE Conference on Electromagnetic Field Computation*. Miami: CEFC, 2016, pp. 1–1. DOI: https://doi.org/10.1109/CEFC.2016.7815883.